Chapter 6
Experimental Results

Upon completion of the computational fillet optimization studies, the linear off-stagnation fillet, described in Figure 6.1, was selected for experimental verification in the wind tunnel vane cascade located in the Virginia Tech Experimental and Computational Convection Laboratory. While the details of the experimental setup and methodology are given in Chapter 4, this chapter presents the experimental results. Four different test conditions, summarized in Table 4.3, were investigated to evaluate the effectiveness and robustness of the fillet in reducing endwall adiabatic temperature levels relative to a baseline unfilleted vane. Two of the tested inlet conditions were without slot coolant injection, while the remaining two were for two different slot blowing ratios. For testing without the backward-facing slot, the thermal performance of the fillet was evaluated for two different inlet total pressure profiles. Both profiles feature a near-wall peak in total pressure, which is characteristic of typical combustor exit conditions. To determine fillet robustness and performance sensitivity to inlet pressure profile, the nominal or design profile peak was roughly doubled for the second tested inlet condition. For testing with the backward-facing slot, the inlet total pressure profile was held fixed at the design condition while the flow rate of coolant exiting the slot was varied. The coolant flow rate was approximately doubled from the design value by increasing the number of coolant feed holes supplying the slot. For each inlet condition considered, baseline tests were conducted without the fillet to provide a means of comparison for the fillet results. The primary measurements performed to evaluate fillet performance were endwall temperature measurements and thermal field measurements.

6.1 Thermal Performance of Fillet for Design Conditions with No Slot

The first inlet condition investigated was the design condition ($\Delta p_{o,max} \approx 1$) without the backward-facing slot. In the computational studies presented in Chapter 5, a comparison between an elliptical and linear fillet was performed for this inlet condition. From the results of that comparison, which indicated better thermal performance for the linear fillet, the linear fillet was selected for experimental verification. To accommodate testing at this inlet condition, the combustor simulator was reconfigured, removing the

backward-facing slot. The slotless configuration is illustrated in Figure 4.13 of Chapter 4.

Measured near-wall inlet temperature distributions both with and without the leading edge fillet for the design conditions ($\Delta p_{o,max} \approx 1$) are presented in Figure 6.2. These measurements were taken at an axial location that corresponds with the leading edge of the fillet, approximately 10 cm upstream of the vane geometric stagnation (X/C = -0.16). The linear thermocouple rake, described in Chapter 4, was used for the measurements, and was positioned on its side such that the elements were aligned in the spanwise vertical direction. The rake was then traversed in the pitchwise Y direction to record the inlet thermal field. The temperature distributions indicate distinct regions of cooler fluid adjacent to the endwall corresponding to the individual coolant jets emanating from the final two rows of cooling holes on the last combustor simulator liner panel. The measurement plane is approximately 10 cooling hole diameters downstream of the last row of holes. The measured inlet profiles are extremely similar with comparable levels of nondimensional temperature. With only slight differences between the measured temperature distributions, the leading edge fillet is shown to have a negligible effect on the inlet thermal field.

Measured endwall adiabatic effectiveness levels for the baseline unfilleted vane are shown in Figure 6.3. The baseline results indicate migration of coolant toward the suction side endwall corner in both vane passages. This migration of coolant is anticipated due to the endwall crossflow present in the passage. The peak effectiveness values observed for the two passages agree at roughly 0.6, however, the inner (upper) passage is shown to have slightly lower effectiveness in the pressure side endwall corner. Despite attempts to improve thermal periodicity between passages, the root cause remained elusive. For this reason, baseline to filleted vane comparisons are always made between like passages. In addition to the difference in minimum effectiveness level, the outer (lower) passage is shown to have slightly broader coolant coverage at the inlet to the vane passage.

The endwall adiabatic effectiveness levels for the filleted vane are shown in Figure 6.4. The peak effectiveness level observed for the baseline case is shown to penetrate further into the passage with the addition of the fillet. The region of low

effectiveness in the pressure side corner is also shown to be significantly reduced in size. Despite the fillet's height in the spanwise direction, which exposes the fillet to higher temperatures as a result of the inlet thermal field, improved thermal protection is observed about the vane leading edge. Similar to the baseline results, slight thermal non-periodicity occurs with broader coolant coverage in the outer passage. To assess repeatability of the results, the data were retaken 20 days after the results of Figure 6.4. The repeated endwall adiabatic effectiveness measurements are presented in Figure 6.5. Excellent agreement with the initial measurements is shown. The primary differences observed are a slightly larger region of low effectiveness in the inner passage and increased penetration of coolant in the outer passage.

To quantify the thermal improvement attributable to the fillet, lateral-averaged values of adiabatic effectiveness were calculated at various axial locations through the vane passage. The results for the initial and repeated data sets are presented in Figures 6.6 and 6.7, respectively. Due to the slight non-periodic thermal field mentioned above, separate lateral-average effectiveness values were calculated for the inner and outer passages. Both figures indicate consistent thermal improvement with the addition of the fillet at all axial positions for both vane passages. In the region upstream of the vane leading edge, effectiveness levels are observed to decay monotonically as one might expect. Interestingly, the upstream rate of decay in effectiveness is greater with the fillet than without it. This is attributed to the influence of the fillet on the lateral spread of coolant in this region. Due to the fillet's presence, the near-wall coolant flow is channeled around the fillet resulting is decreased lateral spreading. This channeling effect of the fillet is much more pronounced in the results with slot coolant injection, presented later in this chapter. Upon entering the passage, lateral-averaged effectiveness levels flatten out. For the filleted vane, a slight increase in effectiveness is observed for the inner passage between X/C = 0.12 and 0.22. A more significant increase is shown for the outer passage fillet results, peaking at X/C = 0.28. These local peaks in effectiveness correspond to where the maximum levels of adiabatic effectiveness intersect the vane suction surface. Beyond this point in the vane passage, lateral-averaged effectiveness continues on a downward trend.

From the lateral-averaged effectiveness results, fillet percentage improvement over the baseline result was calculated for all axial locations as given by equation 6.1

$$\frac{\overline{\eta}_{\text{fillet}} - \overline{\eta}_{\text{baseline}}}{\overline{\eta}_{\text{baseline}}} \times 100 \tag{6.1}$$

The results for the initial and repeated data sets are presented in Figures 6.8 and 6.9, respectively. For the initial data set, percentage improvement is shown to decrease in the region of the endwall upstream of the vane leading edge. This trend is attributed to the greater rate of decay in lateral average effectiveness with the fillet, noted above. Early in the vane passage, percentage improvement begins to increase and continues on an upward trend until the point of coolant intersection with the vane suction surface. Beyond this point the results for the inner and outer passages vary. For the inner passage, percentage improvement is shown to decrease between X/C = 0.22 and 0.30, and finally increase between X/C = 0.30 and 0.38, beyond which data was unavailable. For the outer vane passage, the upward trend continues up to X/C = 0.38, where percentage improvement levels out at approximately 17%. The results for the repeated data set, shown in Figure 6.9, are similar to those of the initial data set with one notable exception. For the outer vane passage, percentage improvement is shown to decay beyond X/C = 0.28 rather than continuing on an upward trend. The differences between the passages are attributed to the thermal non-periodicity discussed previously. In addition, slight geometric variation between the inner and outer passages due to the use of a flexible wall in the outer passage could also contribute to the observed differences.

To evaluate the influence of the fillet on the passage thermal field, temperature measurements were performed in the SS2 plane oriented normal to the vane suction surface. Thermal field measurements were only taken in the inner passage due to difficulties in extending the thermocouple rake to the outer passage. A comparison between the thermal fields of the baseline and filleted vane is presented in Figure 6.10. The baseline thermal field indicates accumulation of coolant in the suction side endwall corner as observed in the endwall effectiveness distributions. Undercutting of the coolant due to the passage vortex is clearly apparent adjacent to the pressure surface.

Additionally, a region of lower effectiveness is present in the suction side endwall corner. This region is also present in the baseline endwall effectiveness contours of Figure 6.3. With the addition of the fillet, the thermal field indicates enhanced coolant coverage up the vane suction surface. Despite this coverage enhancement, the thermal field adjacent to the pressure surface remains essentially unchanged. On the endwall and fillet surfaces, the fillet resulted in a slightly broader region of maximum effectiveness and eliminates the low effectiveness region in the suction side endwall corner.

In summary, the addition of the leading edge fillet has a positive impact on the endwall temperature distribution as well as on the passage thermal field for the design inlet total pressure profile. The fillet results in improved coolant penetration into the vane passage and a reduction in size of the region of low effectiveness. Despite the fillet's height in the spanwise direction, improved thermal protection is observed about the vane leading edge. Lateral-averaged adiabatic effectiveness values indicate consistent thermal performance improvement at all axial locations with the fillet. Percentage improvement in effectiveness ranged between approximately 8% and 17% for the outer passage and between 4% and 12% for the inner passage. Area-weighted average effectiveness values and percentage improvement were also calculated for the design inlet condition and are presented in Table 6.1. An average improvement in endwall adiabatic effectiveness of 9.5% was calculated with the fillet for the design inlet condition. Additional thermal benefit to the vane suction surface was observed from the thermal field results in the SS2 plane.

6.2 Thermal Performance of Fillet for Off-Design Conditions with No Slot

To evaluate the sensitivity of fillet thermal performance to the inlet total pressure profile, an off-design profile was generated through adjustment of the various combustor simulator flows, whereby the near-wall peak in total pressure was increased by a factor of two. In this section, the influence of the fillet on endwall effectiveness levels and the thermal field for off-design inlet conditions is presented first through comparison of baseline and filleted results. Then, comparison of the results with those for the design inlet total pressure profile is made to evaluate fillet robustness.

To achieve the off-design inlet total pressure profile, the mass flow rates exiting the various combustor liner panels and dilution holes were adjusted as indicated in Table 4.1. Specifically, the mass flow rates exiting the last two liner panels were increased, while the flow exiting the first two panels was completely shut off. Since the flow and thermal fields exiting the combustor simulator are inherently linked, altering the inlet total pressure profile also results in a change to the inlet thermal field. The measured inlet near-wall temperature distributions for the off-design total pressure profile are shown in Figure 6.11 for both the baseline and filleted vanes. Both temperature distributions feature distinct regions of lower fluid temperature (higher nondimensional temperature) corresponding to the last two rows of film cooling holes on the upstream liner panel. Slightly lower temperature values are observed for the last row of film holes due to closer proximity to the thermal field measurement plane, which is located approximately 10 hole diameters downstream. In comparison to the measured thermal field for the design inlet total pressure profile, the peaks in nondimensional temperature in this case are not as high. At first, this came as a surprise considering the increase in coolant flow exiting the upstream combustor liner panel; however, in increasing the coolant mass flow, the momentum flux ratio of the coolant jets were also significantly increased, especially for panel 3. It is believed that these increases in momentum flux ratio result in enhanced mixing in the near-wall region. Despite increased coolant mass flow, enhanced mixing of the coolant with the freestream results in lower peak nondimensional temperature. Similar to the measured inlet temperature distributions for the design inlet total pressure profile, the fillet is observed to have negligible impact on the approaching thermal field.

Baseline endwall adiabatic effectiveness levels for the off-design total pressure profile are presented in Figure 6.12. The baseline results indicate lower effectiveness through the center of the vane passage with a region of higher effectiveness wrapped about the vane leading edge. The familiar migration of coolant toward the suction side endwall corner is not as readily apparent. Peak effectiveness levels in the leading edge region between 0.50 and 0.55 are observed for both inner and outer passages. Similar to the results for the design inlet total pressure profile, slight thermal non-periodicity is indicated with lower effectiveness levels in the inner vane passage.

Endwall adiabatic effectiveness levels with the addition of the fillet for the off-design inlet total pressure profile are shown in Figure 6.13. With the fillet, the region of lower effectiveness observed through the center of the passage for the baseline has relocated to the pressure side-endwall corner and increased in size. Instead of wrapping about the vane leading edge, the coolant follows the more familiar path across the passage to the suction side-endwall corner. Effectiveness levels about the trailing edge of the vane have decreased slightly relative to the baseline results.

Comparison of the axial distributions of lateral-averaged effectiveness between the baseline and filleted vanes is presented in Figure 6.14. From the plot, the fillet is not shown to have a significant positive or negative effect on endwall effectiveness levels. Over a relatively small axial range, between X/C of 0.18 and 0.30 for the inner passage and X/C of 0.18 and 0.38 for the outer passage, a slight thermal benefit is measured. Percentage improvement results are presented in Figure 6.15. Consistent with the lateral-averaged effectiveness plot, percentage improvement is slightly negative in the leading edge region and in the upstream portion of the passage. Regardless of the negative influence of the fillet in this region, the general shapes of the percentage improvement curves are remarkably similar to those for the design inlet total pressure profile. Similar peaks in percentage improvement are shown at X/C = 0.22 for the inner passage and X/C = 0.28 for the outer passage. Despite the similarities, one would expect a net negative fillet impact upon integration of the result. Averaging the results for the two passages, a comparison of percentage improvement between the design and off-design inlet total pressure profiles is presented in Figure 6.16. Area-weighted average effectiveness levels for the off-design inlet condition were calculated for both passages and are presented in Table 6.1. A 1.7% reduction in endwall adiabatic effectiveness with the fillet was calculated for the off-design inlet condition, compared to the 9.5% improvement calculated for the design inlet condition.

Temperature measurements were performed in the SS2 plane to evaluate the influence of the fillet on the passage thermal field. A comparison between the thermal fields for the baseline and filleted vanes is given in Figure 6.17. The baseline thermal field indicates accumulation of coolant in the suction side-endwall corner with higher flow temperatures in the pressure side corner. Positive upturning of the isotherms

adjacent to the pressure and suction surfaces indicate the migration of cooler fluid up the vane surface. The results with the fillet indicate accumulation of coolant on the fillet surface with similar effectiveness to that observed for the baseline. The most notable improvement with the fillet is better thermal protection up the suction surface of the vane. The fillet acts to transport cooler fluid up the suction surface.

In summary, the leading edge fillet was observed to have slightly negative overall impact on the endwall temperature distribution for the off-design conditions; however, passage thermal field results indicate a thermal benefit for the vane suction surface. Lateral-averaged adiabatic effectiveness values showed mixed fillet performance through the vane passage. In the upstream leading edge region, the fillet has a negative impact on lateral-averaged effectiveness with reductions around 2 to 4%, while slight thermal improvement is observed over a relatively small axial range midway through the vane passage. From the thermal field results in the SS2 plane, the fillet is shown to have a positive impact on the suction surface with the displacement of cooler fluid up the vane surface.

6.3 Stagnation Plane Flow Field Measurements

Flow field measurements in the stagnation plane of the center vane of the cascade were performed using the two-component LDV system described in Chapter 4 for the original combustor simulator configuration with backward-facing slot coolant injection. The purpose of the measurements was to evaluate the developing secondary flow field for the design inlet total pressure profile. The flow field measurements presented herein were the first taken with the addition of the combustor simulator. Previous flow field measurements in the stagnation plane were performed by Kang et al. (1999) for a turbulent boundary layer inlet condition. However, with the addition of the combustor simulator, the inlet boundary condition to the turbine vane cascade represents a significant departure from a turbulent boundary layer. The combustor simulator flow settings were nominally the same as the design settings of this investigation.

Mean flow field vectors are presented in Figure 6.18. The vectors indicate a near-wall peak in velocity with a local minimum occurring between the peak and midspan. This measured velocity profile parallels the measured inlet total pressure profile

presented in Figure 3.15. The higher velocities measured in the near-wall region are due to coolant injection through the combustor liner panels as well as flow acceleration in the convergent section of the simulator. As the flow passes over the lip of the slot, the spanwise component of velocity (W) goes negative indicating down-turning of the flow into the vane endwall junction. Due to limited optical access, it was not possible to take flow measurements below the lip of the slot. Based on the measurements taken and CFD results for this configuration (Stitzel, 2001), shown in Figure 3.17, it is concluded that a confined vortical structure is present below the lip of the slot.

The influence of the inlet total pressure profile is evident in the measurements nearest the vane leading edge. Along the vane leading edge, a flow split is observed at a spanwise location corresponding to the peak in total pressure. At this location, not only is there down-turning of the flow toward the endwall due to the peak in total pressure, but there is also up-turning of the flow toward midspan. In addition to the flow split, an impingement region is also indicated by the velocity vectors along the vane leading edge at approximately Z/S = 0.25. This region is the result of the local minimum in total pressure that exists between midspan and the near-wall peak. Contours of turbulence intensity for the stagnation plane are presented in Figure 6.19. For the majority of the flow plane, turbulence intensity ranges between 15 and 20%. Slightly elevated intensity levels are observed in the region of peak total pressure; however, more significant increases are observed along the vane leading edge in the region of flow impingement, as well as at the top edge of the slot. The high turbulence levels along the leading edge are believed to be the result of flow instability in the impingement region, as the two opposing flows collide with one another. The flow instability manifests itself as elevated levels of turbulence intensity. In addition, it is believed that the high levels of freestream turbulence may act to augment or amplify the instability. In contrast, turbulence levels in the region of the flow split are nearly equivalent to freestream levels, indicative of a stable flow situation. The elevated turbulence levels adjacent to the top of the slot are believed to be the result of leading edge vortex development and interaction with the slot. To further investigate the dynamics of the flow field, the probability density function (PDF) of spanwise velocity was evaluated at several locations along the span of the vane as shown in Figure 6.20. Near the location of the flow split, the PDF is observed to be

nearly Gaussian with a single peak in the distribution. However, in the impingement region, the PDFs are bimodal indicating that the flow toggles between two preferred states.

6.4 Thermal Performance of Fillet with a Backward-facing Slot

To evaluate the thermal performance of the fillet with slot coolant injection, the interface between the combustor simulator and vane cascade was modified to reintroduce the backward-facing slot. As opposed to altering the combustor simulator configuration, a transition piece between the simulator and cascade was fabricated to accommodate the addition of the slot. The resulting slot geometry is illustrated in Figure 4.14. In comparison to the original slot design, the orientation of the feed holes for the new slot configuration had to be altered due to geometric constraints; however, the number, spacing, and size of the feed holes remained unchanged. Additionally, the spacing between the exit of the slot and the vane leading edge had to be increased to accommodate the linear fillet. The exit of the slot was positioned coincident with the leading edge of the fillet.

With inclusion of the backward-facing slot, the impact of varying slot mass flow on endwall effectiveness was investigated, rather than the influence of inlet total pressure profile. The inlet total pressure profile applied in thermal testing with the slot, as measured above the slot, is similar to the design inlet conditions ($\Delta p_{o,max} \approx 1$). To vary the mass flow rate of coolant exiting the slot, the number of feed holes supplying the slot was increased from 13 for 0.4% slot injection to 27 for roughly 0.8% injection. In this section, the results for the design slot flow rate are presented first, followed by the results for increased slot blowing and comparison between the two.

Baseline endwall adiabatic effectiveness levels for the design slot flow rate (0.4%) configuration are presented in Figure 6.21. Low effectiveness levels are observed around the vane leading edge and in the pressure side endwall corner, indicating down-turning of higher temperature mainstream flow onto the endwall. This down-turning of flow is attributed to the development of the secondary flow system, specifically the leading edge and passage vortices. The coolant exiting the slot is confined to a small

triangular region of high effectiveness and is swept across the passage toward the suction side endwall corner.

The measured endwall adiabatic effectiveness levels with the leading edge fillet are presented in Figure 6.22. With the addition of the fillet, the triangular region of highest effectiveness is actually shown to become somewhat narrower. This is due to the channeling effect of the fillet on the coolant flow exiting the slot. Due to the fillet's presence, the near-wall coolant flow is channeled around the fillet resulting is decreased lateral spreading of the region of peak effectiveness. Despite this channeling effect, improved thermal protection is observed on the fillet adjacent to the vane suction side shoulder. The isotherms in this region have spread out, indicating a reduction in temperature gradient. Similar to the baseline results, the lowest levels of effectiveness occur in the pressure side endwall corner. The filleted results indicate a slight improvement with a reduction in size of the region of minimum effectiveness adjacent to the vane trailing edge.

To quantify the thermal benefit of the fillet, values of lateral-averaged adiabatic effectiveness were calculated throughout the vane passage. Comparison of the lateral-averaged effectiveness between the baseline and filleted vane is presented in Figure 6.23. In the leading edge region upstream of the vane, the filleted results indicate slightly lower effectiveness for both passages. This is attributed to the channeling effect of the fillet on the coolant exiting the slot. A distinct narrowing of the region of peak effectiveness is observed with the addition of the fillet. Despite improved thermal protection on the fillet surface adjacent to the suction side shoulder, the narrowing of the region of peak effectiveness results in a lower lateral average. Shortly into the vane passage (X/C = 0.05), the fillet results begin to show an improvement over the baseline. Continuing through the passage, the improvement in effectiveness increases up to a point, beyond which it diminishes toward the vane trailing edge.

Percentage improvement in lateral-averaged effectiveness as a function of axial position with the addition of the fillet is presented in Figure 6.24. As mentioned above, a slight thermal detriment occurs in the leading edge region due to narrowing of the region of peak effectiveness. Shortly into the vane passage, percentage improvement becomes positive and increasing. Improvement continues to increase up to a point that roughly

corresponds to coolant intersection with the suction surface. For the inner vane passage, this occurs at approximately X/C = 0.2, while for the outer passage, coolant intersection is slightly delayed, occurring at approximately X/C = 0.26. The peak in calculated percentage improvement for both passages is quite similar, at around 12% for the inner passage and slightly less than 11% for the outer passage. In the downstream portion of the vane passage, beyond the point of coolant intersection, percentage improvement in effectiveness decays; however, it does not go negative. Area-weighted average effectiveness levels for both vane passages are presented in Table 6.1. A 2.4% improvement in area-weighted effectiveness with the fillet is indicated for the inner passage, while improvement for the outer passage is calculated to be 1.6%.

A comparison of the measured thermal fields in the SS2 plane between the baseline and filleted vane with 0.4% slot coolant injection is presented in Figure 6.25. The baseline thermal field indicates that the majority of the coolant experiences lift-off, leaving only a small amount of coolant on the endwall for thermal protection. Undercutting of the coolant indicates the presence of the passage and suction side vortices. The mass of coolant displaced from the endwall appears to have two distinct lobes. The smaller lobe adjacent to the suction surface is believed to be the result of the suction side leg of the leading edge horseshoe vortex. With the addition of the fillet, coolant lift-off does not occur. The coolant is observed to accumulate on the fillet surface in the suction side endwall corner, providing thermal protection for the fillet. Mix-out of the coolant has also been reduced with the fillet, as indicated by higher values of nondimensional temperature. This is indicative of a reduction in the turbulence levels which enhance mix-out of the cooling flow. In comparing the flow temperature levels adjacent to the endwall, fillet and vane surfaces, a definite thermal improvement is observed with the fillet. Undercutting of the coolant in the fillet endwall corner may indicate delayed development of the passage vortex.

The results for the design slot flow rate clearly indicate a thermal improvement with the fillet. Though the measured endwall adiabatic effectiveness levels with the leading edge fillet indicated narrowing of the region of peak effectiveness, improved thermal protection was observed adjacent to the vane suction side shoulder. A slight improvement was observed in the pressure side endwall corner. A comparison of lateral

averaged effectiveness distributions indicated a fillet thermal benefit through the majority of the vane passage. A slight thermal detriment occurs in the leading edge region due to the channeling effect of the fillet on the coolant. Peak improvement in effectiveness occurs approximately halfway through the passage and corresponds to the point of coolant intersection with the vane suction surface. Thermal field results in the SS2 plane show a dramatic improvement with the addition of the fillet. Without the fillet, coolant lift-off is observed, leaving only a small amount of coolant on the endwall for thermal protection. With the fillet, coolant lift-off is prevented and higher values of nondimensional temperature are indicative of reduced coolant mix-out. Based on these observations, it is believed that the fillet presents a significant thermal benefit to the first vane.

To quantify the thermal benefit of additional coolant mass flow exiting the slot and to evaluate the sensitivity of fillet performance to changes in slot flow, tests were conducted at nominally twice the design slot flow rate. Baseline endwall adiabatic effectiveness levels for the 0.8% slot flow configuration are presented in Figure 6.26. Similar to the results for the design slot flow rate, low effectiveness levels are observed around the vane leading edge and in the pressure side endwall corner, indicative of secondary flow field development. The coolant exiting the slot is also shown to be confined to a small triangular region of high effectiveness, and is swept across the passage toward the suction side endwall corner. In comparison to the baseline results for the design slot flow rate, shown in Figure 6.21, the region of high effectiveness is slightly larger in extent with improved penetration of coolant into the passage.

The measured endwall adiabatic effectiveness levels with the leading edge fillet are presented in Figure 6.27. These results indicate a similar influence of the fillet to that observed for the design slot flow rate. The region of highest effectiveness is somewhat narrower due to the channeling effect of the fillet on the coolant flow exiting the slot. Improved thermal protection is observed on the fillet adjacent to the suction side shoulder. The distance between isotherms in this region has increased, indicating a reduction in temperature gradient. In comparison to the fillet results for the design slot flow rate in Figure 6.22, the region of peak effectiveness is broader and shows enhanced penetration of coolant into the vane passage.

To further quantify the thermal benefit of the fillet, lateral-averaged adiabatic effectiveness values were calculated through the vane passage. Comparison of the lateral-averaged effectiveness between the baseline and filleted vane is presented in Figure 6.28. In the leading edge region upstream of the vane, the results for both passages indicate slightly lower effectiveness with the fillet. This is attributed to the channeling effect of the fillet on the coolant exiting the slot. Despite improved thermal protection on the fillet surface adjacent to the suction side shoulder, the reduced size of the region of peak effectiveness results in a slightly lower lateral average. Continuing into the vane passage, improved thermal protection is observed over a majority of the endwall. In the exit region, thermal benefit diminishes to nearly zero.

Percentage improvement in lateral-averaged effectiveness with the fillet is presented as a function of axial position in Figure 6.29. As noted from the lateral-averaged effectiveness results, a slight thermal detriment occurs in the leading edge region due to narrowing of the region of peak effectiveness. Percentage improvement becomes positive at approximately X/C = 0.06 for the inner passage and X/C = 0.14 for the outer passage. In comparison to the results for the design (0.4%) slot flow, a larger disparity is shown between the locations of peak improvement for the two passages. For the inner vane passage, peak improvement occurs at approximately X/C = 0.2, similar to the 0.4% slot flow results. However, for the outer vane passage, peak improvement is delayed until X/C = 0.38, though a smaller local peak is shown at X/C = 0.28. The magnitudes of peak percentage improvement for the two passages are not as similar as for 0.4% slot flow. Percentage improvement peaks at slightly more than 11% for the inner passage, but falls just short of 8% for the outer passage. Area-weighted average effectiveness values for the two passages were calculated from the measured endwall distributions and are presented in Table 6.1. Based on the area-weighted results, a 1.1% improvement in effectiveness was calculated for the inner passage, and a 0.5% thermal detriment was calculated for the outer passage.

To visualize the benefit of increased slot flow for the baseline unfilleted vane, the axial distributions of lateral-averaged effectiveness for 0.4% and 0.8% slot flow are plotted for comparison in Figure 6.30. The results for both passages indicate higher effectiveness with increased slot flow at nearly all axial positions. The only exception to

this is in the vane trailing edge region for the outer passage where effectiveness for 0.8% slot flow dips slightly below that for 0.4% slot flow. However, the difference is well within experimental uncertainty, so the effectiveness distributions are considered to be convergent. Percentage improvement in effectiveness for the two passages is presented in Figure 6.31. For both passages, percentage improvement starts high and decays in the region upstream of the vane leading edge. The inner passage shows more improvement, at nearly 20%, than the outer passage at slightly more than 11%, however, the rates of decay are nearly identical. Into the passage, percentage improvement levels out for the inner passage remaining between 8 and 11% until approximately X/C = 0.25. Beyond this axial location, percentage improvement continues to decay. For the outer passage, percentage improvement increases significantly early in the passage to approximately 10%. Similar to the inner passage results, percentage improvement is nearly constant, between 10 and 12%, through a good portion of the passage. Beyond X/C = 0.28, the benefit of increased slot flow begins to decay toward zero.

A similar comparative analysis to that described above was performed for the filleted results at 0.4% and 0.8% slot flow. Figure 6.32 presents the lateral-averaged effectiveness distributions for the two slot flow rates. Similar to the baseline unfilleted results, increased slot flow is shown to yield higher values of lateral-averaged effectiveness throughout the vane passage. The most significant benefit is felt in the region upstream of the vane leading edge. The effectiveness distributions for the outer passage converge in the downstream portion of the passage near the vane trailing edge. To quantify the thermal benefit of increased slot flow, distributions of percentage improvement were calculated as presented in Figure 6.33. The results for the filleted vane are remarkably similar to those for the baseline comparison. Peak values of percentage improvement in the leading edge region are nearly identical to those for the baseline comparison, at approximately 20% for the inner passage and 11% for the outer passage. Similar to the baseline comparison, percentage improvement steadies out in the vane passage between 7 and 9% for the inner passage and 2 and 5% for the outer passage. One distinct difference from the baseline comparison is that the significant increase in improvement observed in the upstream portion of the outer passage does not occur. It is

believed that the uncertainties in the compared results combined in such a way to produce the observed difference.

To compare the performance of the fillet at 0.8% slot flow with fillet performance for 0.4% slot flow, inner and outer passage results were averaged for the two cases and are presented in Figure 6.34. In the leading edge region, the results for the two different slot flow rates are found to be almost identical, differing by less than one percentage point. The two distributions begin to deviate at approximately X/C = 0.05, beyond which they vary by nearly a constant amount. The result for 0.8% slot flow is consistently lower by 4 to 5 percentage points. Both distributions reach a peak around X/C = 0.20. The maximum percentage improvement for 0.4% slot flow is slightly less than 11%, while for 0.8% slot flow the maximum improvement is 6.5%. Though these results suggest better fillet thermal performance for 0.4% slot flow, they agree within experimental uncertainty. The influence of slot flow on fillet thermal performance is therefore considered indeterminate.

A comparison of the measured thermal fields in the SS2 plane between the baseline and filleted vane for 0.8% slot coolant injection is presented in Figure 6.35. Similar to the results for the design (0.4%) slot flow rate, the baseline thermal field indicates coolant lift-off. Only a small amount of coolant remains on the endwall for thermal protection. Undercutting of the coolant on both the pressure and suction sides indicate the presence of the passage and suction side vortices, respectively. In comparison to the design (0.4%) slot flow rate results, higher values of nondimensional temperature are shown due to enhanced coolant penetration at the higher slot flow rate. With the addition of the fillet, coolant lift-off is not observed. Rather, the coolant adheres to the fillet surface in the suction side endwall corner, providing improved thermal protection. Indicative of a reduction in secondary flow strength and subsequent coolant mix-out, higher values of nondimensional temperature are observed with the fillet.

The results for 0.8% slot flow rate unquestionably indicate a thermal improvement with the fillet. A similar influence of the fillet is observed for this configuration as for the design slot flow configuration. Narrowing of the region of peak effectiveness and improved thermal protection adjacent to the vane suction side shoulder are shown with the addition of the fillet. The axial distribution of percentage

improvement in effectiveness is also remarkably similar to that for the design slot flow rate case. Thermal field results in the SS2 plane show a significant thermal improvement with the addition of the fillet. Coolant lift-off is prevented, providing better thermal protection to the fillet and endwall, and higher values of nondimensional temperature are measured, indicating reduced coolant mix-out. Comparison between the 0.4% and 0.8% slot flow results indicate enhanced thermal protection for the higher slot flow rate.

6.5 Comparison of Experimental and Computational Results

In order to assess the accuracy of computational predictions, comparison must be made to experimental data for similar geometry and boundary conditions. Most often, such comparison is incomplete at best due to limited experimental data. Due to the expense of time and money inherent to acquiring data, it is crucial for the experimenter to choose wisely the data necessary for reasonable comparison. In this study, initial computational results provided guidance on the choice of experimental verification data. The SS2 flow plane was chosen for thermal field measurement as it proved to be a good indicator of fillet performance in the preliminary computations.

In addition to measurement in the SS2 plane, temperature measurements were also performed in the near-wall region upstream of the vane leading edge to verify the thermal field entering the vane cascade. These inlet thermal field measurements, discussed earlier in this chapter, are presented in Figures 6.3 and 6.12 for the design and off-design inlet total pressure profiles, respectively. Though originally intended to investigate the influence of the fillet on the approaching thermal field, these measurements proved to be extremely important for comparison of experimental and computational results. Upon comparison of this data to the computational prediction at the same location, it was discovered that the computations predicted significantly less thermal diffusion and coolant mix-out than actually occurs. This mismatch between experiment and prediction is believed to be due to the manner in which coolant is introduced into the combustor simulator. While the specified computational inlet boundary condition is two dimensional with no variation in the pitchwise direction, the coolant is introduced through discrete film holes in the simulator, thereby enhancing coolant mix-out. Further augmenting mixing, turbulence levels at the inlet to the vane

cascade are between 15 and 18%, as previously reported by Barringer at al. (2002). To correct for the thermal mismatch, a value of coolant temperature was chosen for the computations such that the predicted nondimensional temperature profile at the vane inlet agreed with the measurements. Comparisons of the computational and measured spanwise temperature profiles are presented in Figures 3.19 and 3.22 for the design and off-design inlet total pressure conditions, respectively. The chosen values of coolant temperature to achieve nondimensional similitude are given in Table 3.2.

In addition to limited availability of experimental data for comparison, the modeling assumptions made in the computations are another common deficiency in comparing computations with measurements. Due to limited computational resources, simplifying assumptions are frequently made in modeling a flow situation. In making such assumptions, it is the hope of the computationalist that the physics of the problem are not dramatically altered, though it is acknowledged that assumptions invariably affect the result. Assessing the acceptability of a particular modeling assumption is largely a matter of experience. Several simplifying assumptions were made for the computations performed in this investigation. First, the applied inlet boundary conditions were assumed uniform in the pitchwise (circumferential) direction, varying only in the spanwise (radial) direction. Though this is not precisely correct for the exit conditions of the combustor simulator, it is considered a reasonable assumption. To simplify solution domain geometry generation and meshing, several features of the backward-facing slot were omitted. Instead of modeling the individual slot feed holes and the pin fin array, the slot was assumed to be two-dimensional with uniform inlet velocity and temperature. Additional features omitted in the computational geometry are the upstream contraction of the combustor simulator and coolant injection through the last liner panel. In addition to simplifications of boundary conditions and model geometry, the turbulence modeling approach can also have a significant impact on the accuracy of computational results. Successfully benchmarked by Hermanson and Thole (1999), the RNG k-ε model was used in this investigation in conjunction with wall functions to model the near-wall region.

Regardless of the simplifying assumptions and limited experimental data, comparison of computational and experimental results is essential for qualification of a

computational code and modeling approach. In this section, the measured and predicted thermal fields in the SS2 plane are compared for the design and off-design experimental conditions without the backward-facing slot. Comparison between the endwall adiabatic effectiveness distributions is presented, followed by comparison of measured and predicted distributions of lateral-averaged effectiveness and percentage improvement in effectiveness. Finally, thermal field results for the design (0.4%) slot flow configuration are compared to the computational results for an elliptical fillet with coolant injection through a backward-facing slot.

Comparison between the measured and predicted thermal fields in SS2 for the baseline unfilleted vane at design inlet conditions ($\Delta p_{o,max} \approx 1$) is presented in Figure 6.36. The experimental results indicate accumulation of coolant in the suction side endwall corner, while the computational results show more uniform coolant coverage on the endwall. It appears that the effect of the passage vortex was under-predicted leading to limited redistribution of the thermal field. Another notable difference between the thermal fields is the extent of coolant transport up the vane pressure surface. Such transport is attributed to the counter rotating vortex that resides above the passage vortex, as shown in the baseline results of Figure 5.30. The experimental results indicate less coolant migration up the pressure surface, indicating possible over-prediction of counter-rotating vortex strength. Measured coolant transport up the vane suction surface is in better agreement with prediction.

Comparison of the baseline measured and predicted endwall adiabatic effectiveness distributions for the design inlet condition is presented in Figure 6.37. The predicted levels of adiabatic effectiveness do not exhibit as much variation across the passage as observed experimentally. In addition, the predicted inlet thermal field is much more uniform than the measured thermal field. These differences are believed to be due to enhanced mix-out of the injected coolant in the experiments, as well as, slight under-prediction of secondary flow development through the vane passage.

Thermal field comparison between computational and experimental results with the fillet is presented in Figure 6.38. In agreement with the baseline comparison, measured coolant coverage on the endwall is not as uniform as predicted. While the computational flow field results, shown in Figure 5.31, indicate elimination of a coherent

passage vortex with the fillet, the experimental thermal field measurements seem to suggest that a passage vortex may be present. Since the fillet does not eliminate the cross-passage pressure gradient, it stands to reason that endwall crossflow is present and that a passage vortex may develop. Transport of cooler fluid up the vane pressure and suction surfaces is shown in the experimental measurements. Agreement with prediction is remarkably good up the suction surface; however, similar to the baseline comparison, agreement is poor for the pressure surface. The differences between the thermal fields are believed to be due to over-prediction of counter-rotating vortex strength and under-prediction of endwall crossflow or passage vortex strength.

Comparison between the predicted and measured distributions of endwall adiabatic effectiveness with the fillet for the design inlet condition is presented in Figure 6.39. Similar to the baseline comparison, the predicted effectiveness distribution shows less cross-passage variation than the measurements, and the predicted inlet thermal field is more uniform in the pitchwise direction. Differences are attributed to enhanced coolant mix-out in the experiments and possible under-prediction of passage vortex strength.

The measured and predicted axial distributions of lateral-averaged adiabatic effectiveness are presented in Figure 6.40. Similar levels of effectiveness were calculated for the computational results as for the experimental measurements; however, the difference between the predicted baseline and filleted results is not as significant as the measured differences between baseline and filleted vanes. The computational effectiveness distributions are nearly identical in the leading edge region, diverge slightly through the passage, and then begin to reconverge near the vane trailing edge. Percentage improvement in lateral-averaged effectiveness with the fillet is plotted in Figure 6.41 for the computational and experimental results. The computational results are shown to significantly under-predict measured fillet thermal benefit. Despite the under-prediction, the predicted distribution of thermal improvement exhibits the commonly observed trend of increasing benefit into the vane passage, followed by diminishing benefit in the latter portion of the passage. Area-weighted average endwall effectiveness values are tabulated in Table 6.1 for both experimental and computational results at the design inlet condition. The experimental results indicate a 9.5% average

improvement in effectiveness, while the computations yield a 1.5% average improvement.

Comparison between the measured and predicted baseline thermal fields in SS2 for the off-design inlet total pressure profile ($\Delta p_{o,max} \approx 2$) is presented in Figure 6.42. Similar to the results for the design inlet total pressure profile, the measured thermal field indicates accumulation of coolant in the suction side endwall corner, while the computations predict more uniform coolant coverage on the endwall. Due to the increased near-wall peak in total pressure, enhanced transport of cooler fluid up the vane surfaces is predicted. Substantiating this prediction, the same trend is evident through comparison of the measured thermal fields for the two inlet total pressure profiles. From a fillet design perspective, it is especially significant that CFD predicts the same trend, despite differences with the measurements.

Figure 6.43 presents a comparison of the adiabatic effectiveness distributions between baseline measurement and prediction for the off-design inlet condition. Similar to the thermal field results discussed above, the computations predict more uniform coolant coverage on the endwall. Throughout the vane passage, pitchwise variation of effectiveness is under-predicted. This is believed to be attributed to under-prediction of passage vortex development and associated redistribution of the thermal field. Upstream of the vane passage, the predicted inlet thermal field is also shown to be more uniform compared to experimental results. The uniformity of the predicted thermal field is believed to be the result of the pitchwise invariant inlet temperature profile applied in the computations.

Figure 6.44 compares the measured and predicted thermal fields with the fillet for the off-design inlet total pressure profile. Similar to the baseline comparison, measured coolant coverage on the endwall is not as uniform as shown for the computations. The computations predict enhanced transport of cooler fluid up the vane pressure and suction surfaces relative to the baseline. Supporting this predicted trend, the measured thermal field with the fillet also shows increased transport of cooler fluid up the suction surface; however, the thermal field adjacent to the pressure surface gives no indication of enhancement. As for the design inlet condition results, the observed thermal field

differences are believed to be due to over-prediction of counter-rotating vortex strength and under-prediction of endwall crossflow or passage vortex strength.

Comparison between the predicted and measured distributions of endwall adiabatic effectiveness is presented in Figure 6.45 for the filleted vane at the off-design inlet condition. Once again, the computations indicate less variation in effectiveness upstream of the vane and throughout the passage. These differences are attributed to the pitchwise uniformity of the inlet temperature profile and under-prediction of secondary flow development.

The measured and predicted axial distributions of lateral-averaged adiabatic effectiveness for the off-design inlet total pressure profile are presented in Figure 6.46. Slightly higher levels of effectiveness are shown for the computational results compared to those calculated for the experimental measurements. For both computational and experimental results, the difference between baseline and filleted effectiveness distributions is small. Deviation between the computational effectiveness distributions is barely discernable as they diverge only slightly in the passage before collapsing again near the vane trailing edge. To compare the measured and predicted thermal benefit distributions, percentage improvement in lateral-averaged effectiveness with the fillet is plotted against axial distance through the vane passage in Figure 6.47. Unlike the predicted percentage improvement for the design inlet total pressure profile, the computational predictions in this case are more consistent with experimental observation. Similar to the results for the design inlet conditions, the same trend of increasing thermal benefit through the vane passage with decreasing benefit in the latter portion of the passage is shown. The experimental results for both the inner and outer passage exhibit the same trend. Regardless of better agreement between the computations and the experimental measurements, the plot of percentage improvement indicates negligible fillet thermal benefit for the off-design inlet total pressure profile. Area-weighted average values of endwall effectiveness, given in Table 6.1, indicate a 1.7% reduction in effectiveness for the measurements, and a 0.8% improvement in average effectiveness for the computations.

Though computations were not performed for a linear fillet with slot coolant injection, the computational results for an elliptical fillet with slot flow were compared to

the experimental results for 0.4% slot flow with the linear fillet. Figure 6.48 presents the measured and predicted thermal fields in the SS2 plane without a leading edge fillet. Both thermal fields show coolant lift-off from the endwall. However, the measurements indicate that a small amount of coolant remains attached to the endwall which is absent in the prediction. Similar undercutting of the coolant is shown in both results, suggesting the presence of the passage and suction side vortices. Favorable agreement is observed in regard to fluid transport up the suction surface, but transport up the pressure surface appears to be over-predicted.

Comparison between baseline predicted and measured endwall effectiveness distributions for 0.4% slot flow is presented in Figure 6.49. It should be noted that the location of the slot relative to the vane leading edge is different for the prediction and measurements. Computations were performed for the original slot configuration, with the slot located approximately 0.08C upstream of the vane leading edge. To accommodate thermal testing of the linear fillet, the slot was repositioned 0.16C upstream of the vane in the experiments. In comparing the results, the region of peak effectiveness is shown to be much smaller for the prediction, with significantly less coolant penetration into the passage. These observations are indicative of coolant lift-off from the endwall early into the vane passage. While similar coolant lift-off was measured in the experiments, some of the coolant remained attached to the endwall. Due to the attached coolant, higher levels of effectiveness are observed further into the passage for the experiments. The differences between prediction and measurement give indication that the position of the slot relative to the vane leading edge may have a significant impact on coolant effectiveness.

The measured and predicted thermal fields with a fillet are presented in Figure 6.50. The measured thermal field with a linear leading edge fillet indicates attachment of the coolant to the fillet suction surface. The highest recorded value of nondimensional temperature resides adjacent to the fillet surface. In comparison to the baseline measurements, the fillet provides enhanced protection to the endwall and overall higher values of nondimensional temperature. For the predicted thermal field with an elliptical fillet, coolant lift-off is still predicted with the coldest flow temperatures observed away from the endwall and fillet surfaces. Despite lift-off, a thermal benefit is predicted for the

elliptical fillet. It is believed that the elliptical fillet shape is not aggressive enough to ensure coolant attachment.

Comparison between predicted endwall effectiveness results for an elliptical fillet and measured results for a linear fillet is presented in Figure 6.51. Similar to the baseline comparison, the region of peak effectiveness for the prediction is much smaller, and coolant lift-off occurs early in the vane passage. Experimental results for the linear fillet indicate much better coolant distribution over the endwall and fillet surfaces. Despite the improved performance of the linear fillet in preventing coolant lift-off, area-weighted average effectiveness results, summarized in Table 6.1, yield a 3.4% improvement for the elliptical fillet and a 2.0% improvement for the linear fillet.

In summary, comparison of measured and predicted results did not show absolute agreement, however, similar trends were observed for both. For the design and off-design inlet total pressure profiles without the backward-facing slot, experimental measurements indicated cross-passage migration of coolant to the suction side endwall corner. The computations, in contrast, predicted more uniform coolant coverage of the endwall. Both measurements and predictions showed enhanced thermal protection with the fillet up the suction surface of the vane; however, while the computations indicated similar enhancement up the pressure surface, the measurements exhibited little to no change. The differences between the measured and computed thermal fields are attributed to over-prediction of the strength of the counter-rotating vortex and under-prediction of the strength of the cross-passage flow and the passage vortex. It is possible that these predictive shortcomings are a product of the modeling assumptions made in the computations. Specifically, it is plausible that omission of the combustor simulator contraction immediately upstream of the vane cascade could significantly affect the prediction of secondary flow strength. Comparison between measurements and predictions with backward-facing slot coolant injection yielded reasonably good agreement for the baseline results. Baseline experimental and computational thermal fields both indicate detrimental coolant lift-off from the endwall; however, the measurements show a small amount of coolant remaining on the endwall which is absent in the prediction. Comparison between the measured thermal field with a linear fillet and the predicted thermal field for an elliptical fillet showed a distinct difference between the

two. The linear fillet was observed to promote coolant attachment, while the elliptical fillet result still predicted coolant lift-off. Disagreement between the thermal fields is attributed to the difference in fillet shape.

Table 6.1 Summary of measured and predicted area-average effectiveness for the tested conditions.

Inlet Condition	Baseline		Filleted		% Improvement with the Fillet		
	Inner Passage	Outer Passage	Inner Passage	Outer Passage	Inner Passage	Outer Passage	Average
Design ($\Delta p_{o,max} \approx 1$)	0.445	0.475	0.472	0.536	6.2	12.8	9.5
Design CFD	0.521		0.529		1.5		
Off-Design ($\Delta p_{o,max} \approx 2$)	0.437	0.448	0.429	0.442	-2.0	-1.5	-1.7
Off-Design CFD	0.463		0.467		0.8		
0.4% Slot Flow	0.407	0.450	0.417	0.457	2.4	1.6	2.0
0.4% Slot Flow CFD	0.353		0.365		3.4		
0.8% Slot Flow	0.452	0.476	0.456	0.474	1.1	-0.5	0.3

Fillet Design Parameters	
D_{max}/C	0.16
H_{max}/C	0.16
s_{Dmax}/C	0.058
s_{Hmax}/C	0.115
$s_{max,ps}/s_{total,ps}$	0.97
$s_{max,ss}/s_{total,ss}$	0.44

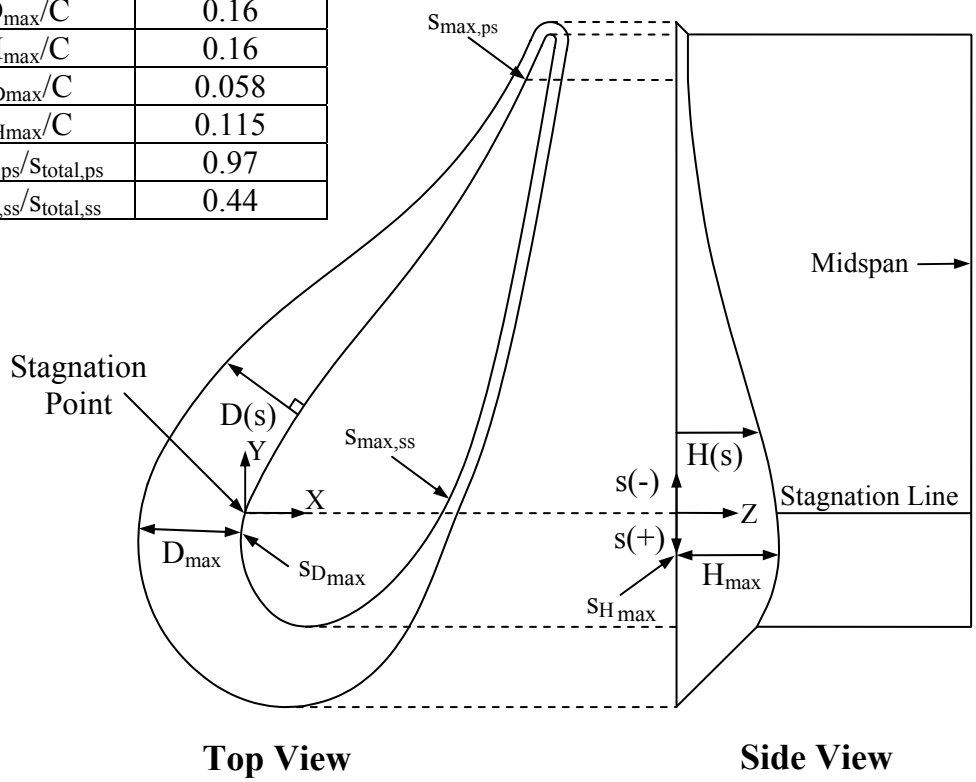

Figure 6.1 Leading edge fillet design tested in the low-speed vane cascade.

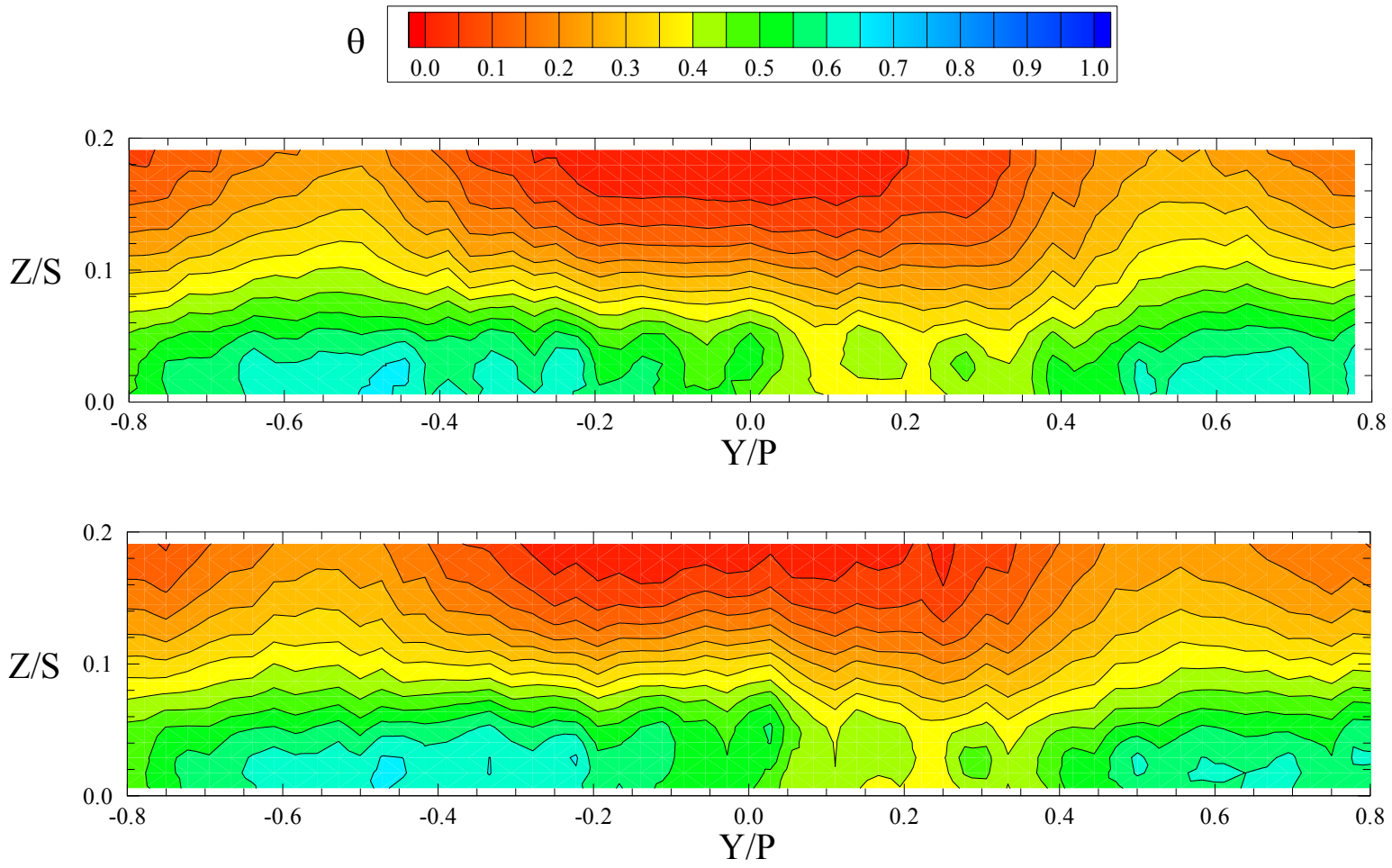

Figure 6.2 Measured inlet near-wall temperature distribution without (top) and with (bottom) the leading edge fillet for the design inlet total pressure profile ($\Delta p_{o,max} \approx 1$). Measurement plane is located approximately 10 hole diameters downstream of the last row of film cooling holes.

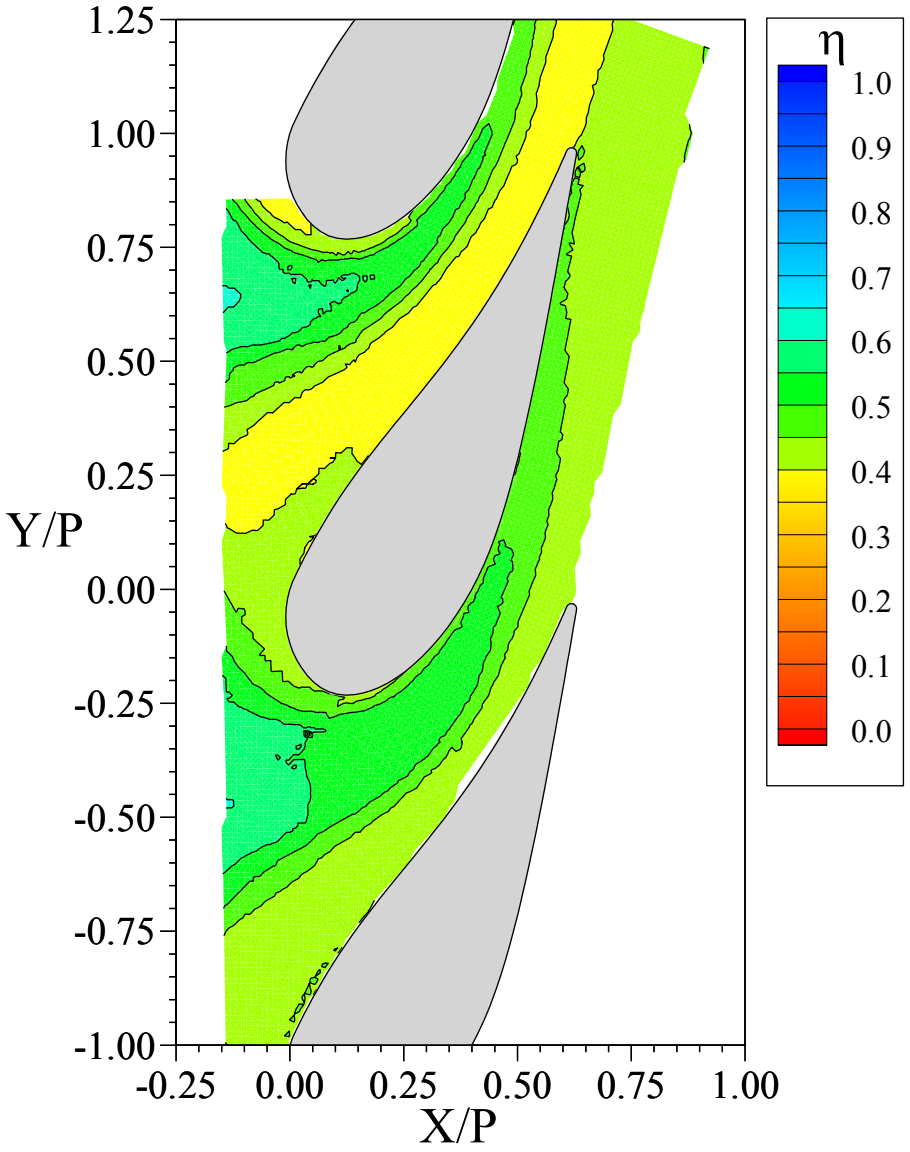

Figure 6.3 Measured endwall adiabatic effectiveness distribution for the baseline, unfilleted vane at the design inlet condition ($\Delta p_{o,max} \approx 1$).

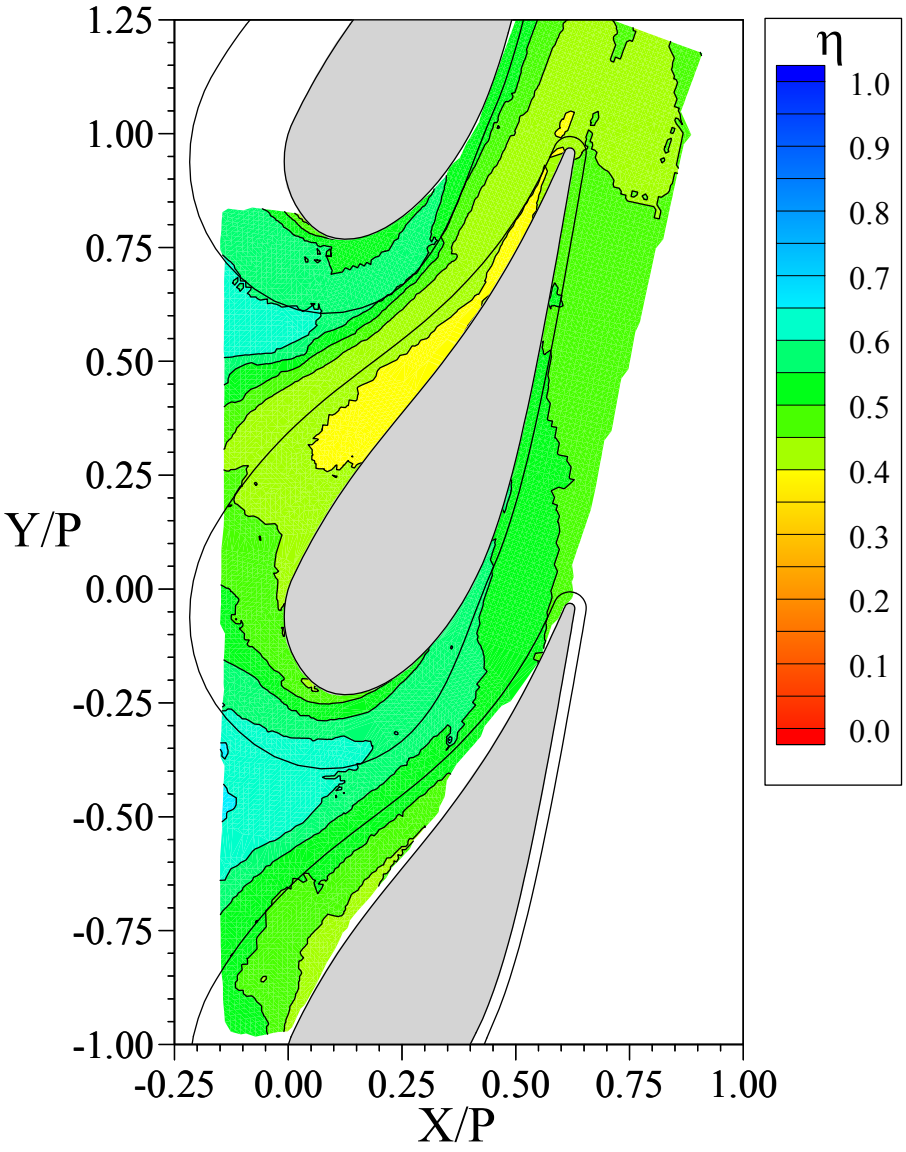

Figure 6.4 Measured endwall adiabatic effectiveness distribution with the fillet at the design inlet condition ($\Delta p_{o,max} \approx 1$).

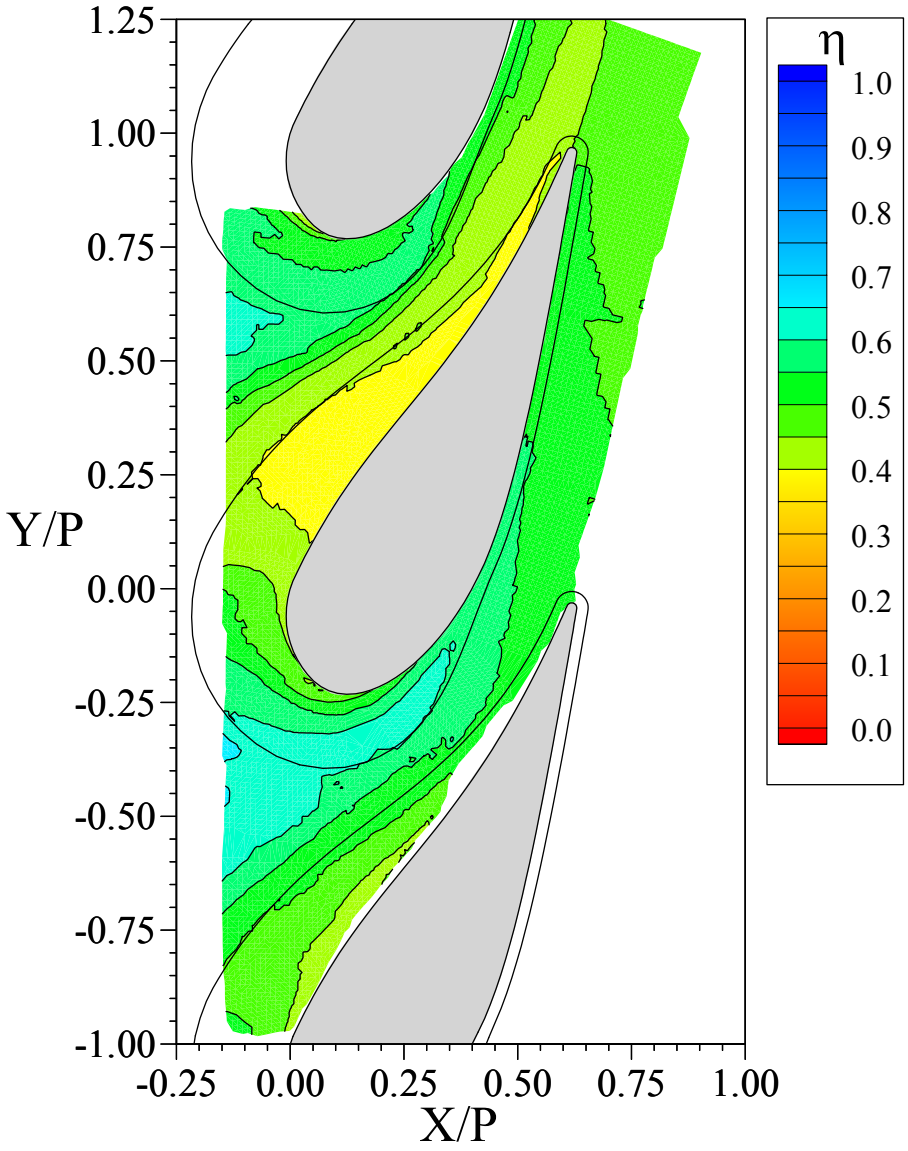

Figure 6.5 Repeated measurement of endwall adiabatic effectiveness distribution with the fillet at the design inlet condition ($\Delta p_{o,max} \approx 1$).

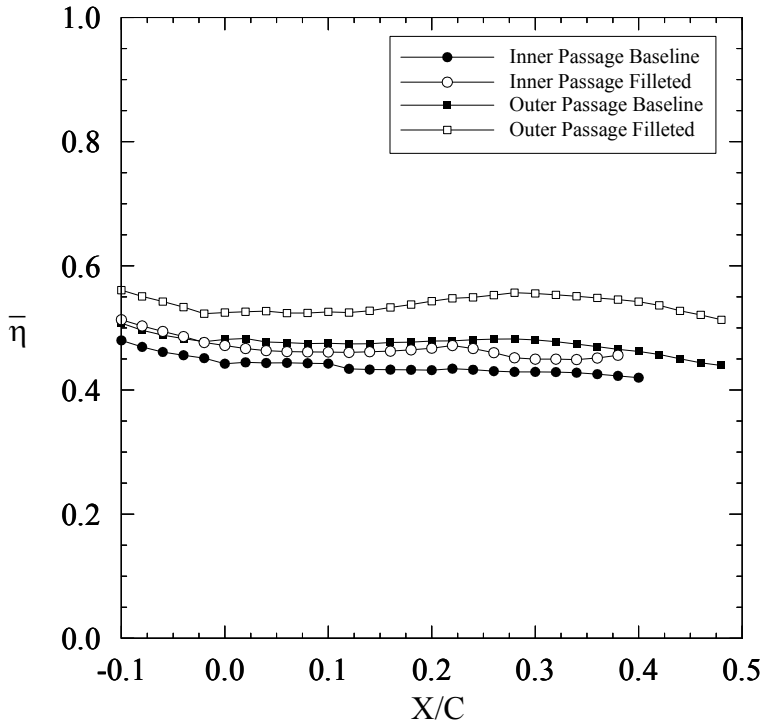

Figure 6.6 Lateral average effectiveness comparison between the baseline and filleted vane for the design inlet condition ($\Delta p_{o,max} \approx 1$).

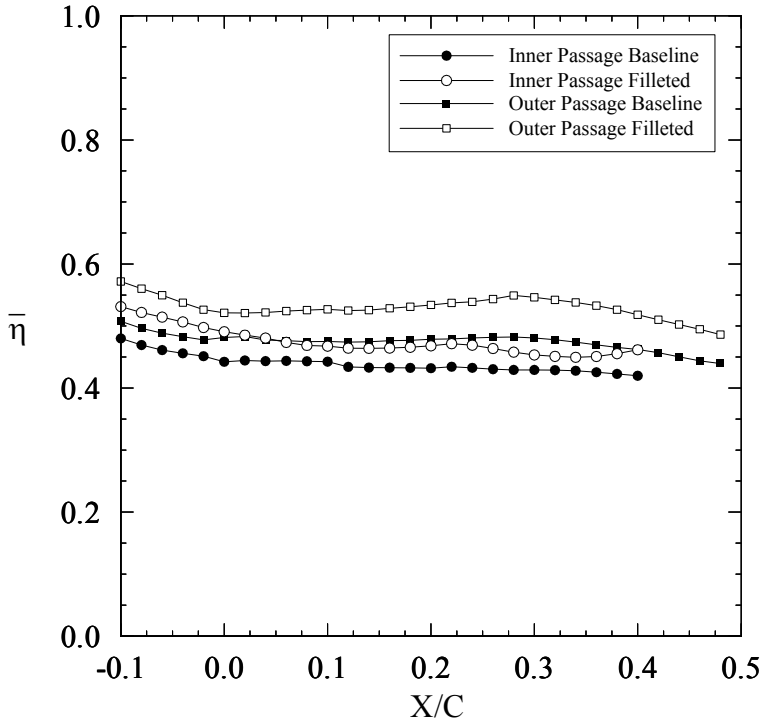

Figure 6.7 Lateral average effectiveness comparison between the baseline and filleted vane for the design inlet condition ($\Delta p_{o,max} \approx 1$). Repeat.

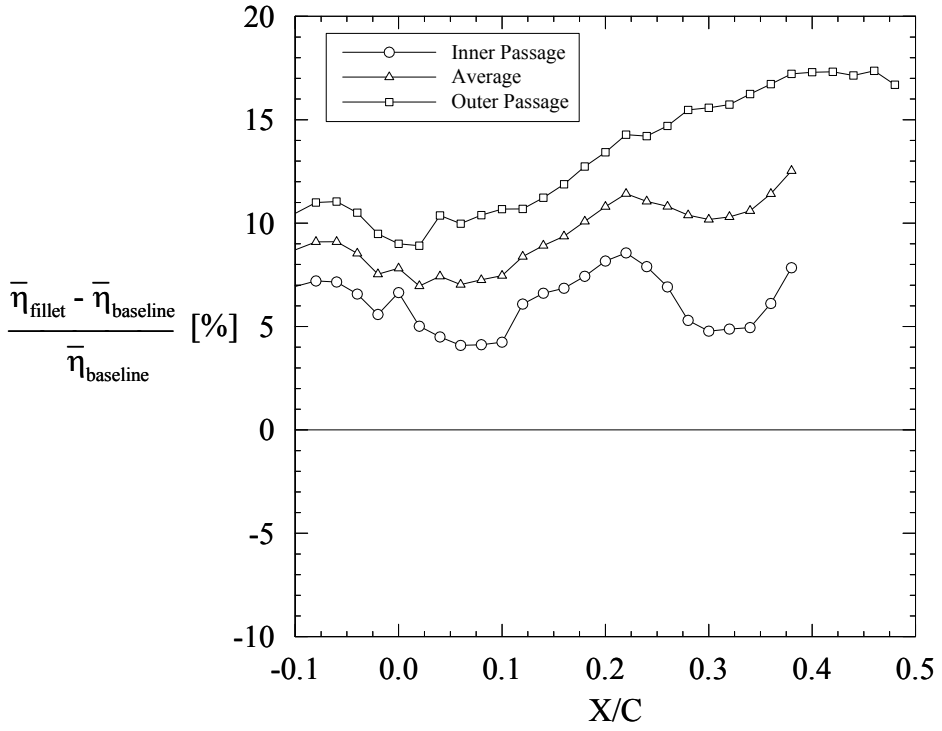

Figure 6.8 Percentage improvement in lateral average effectiveness with the fillet for the design inlet condition ($\Delta p_{o,max} \approx 1$).

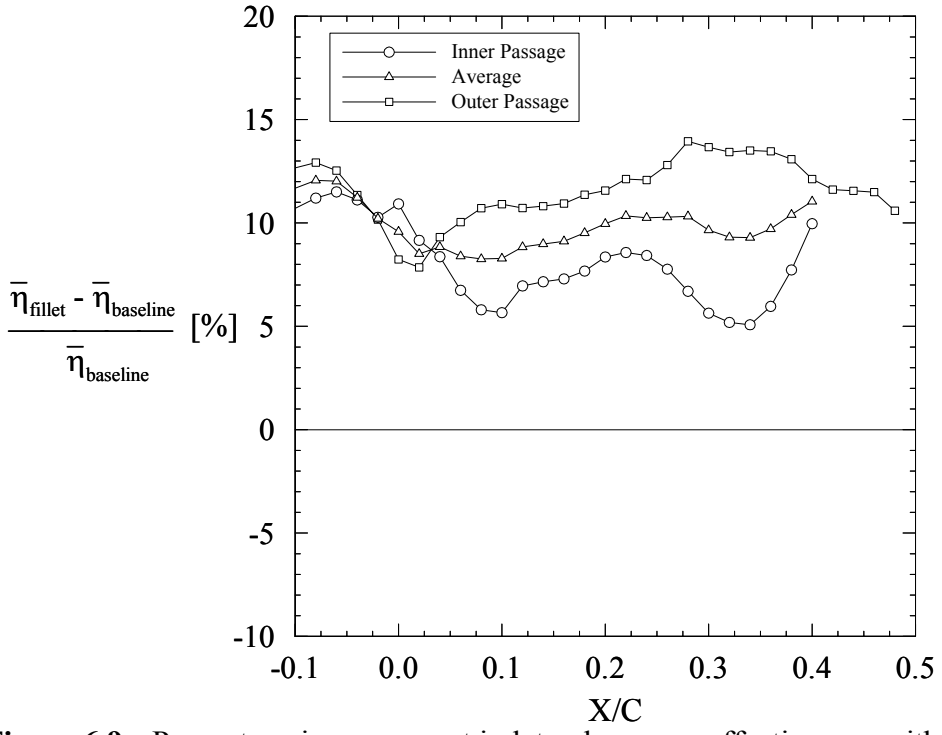

Figure 6.9 Percentage improvement in lateral average effectiveness with the fillet for the design inlet condition ($\Delta p_{o,max} \approx 1$). Repeat.

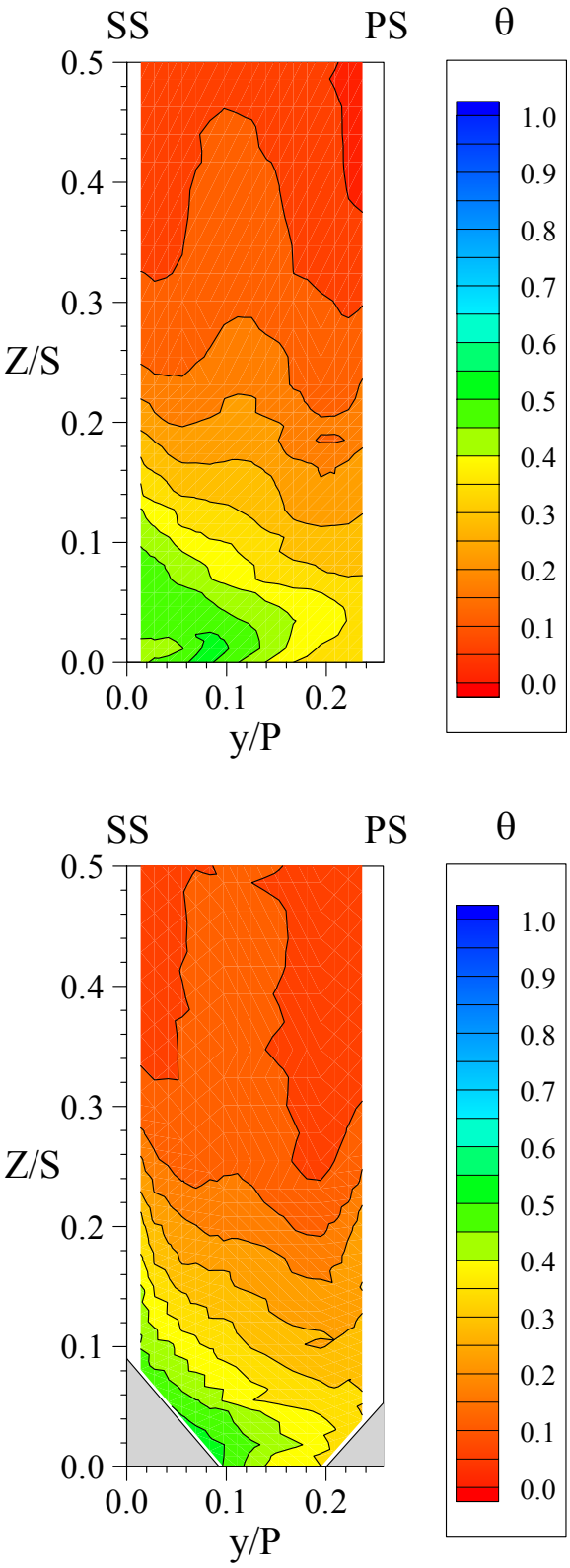

Figure 6.10 Comparison of the thermal field in SS2 between the baseline and filleted vane for the design inlet condition ($\Delta p_{o,max} \approx 1$).

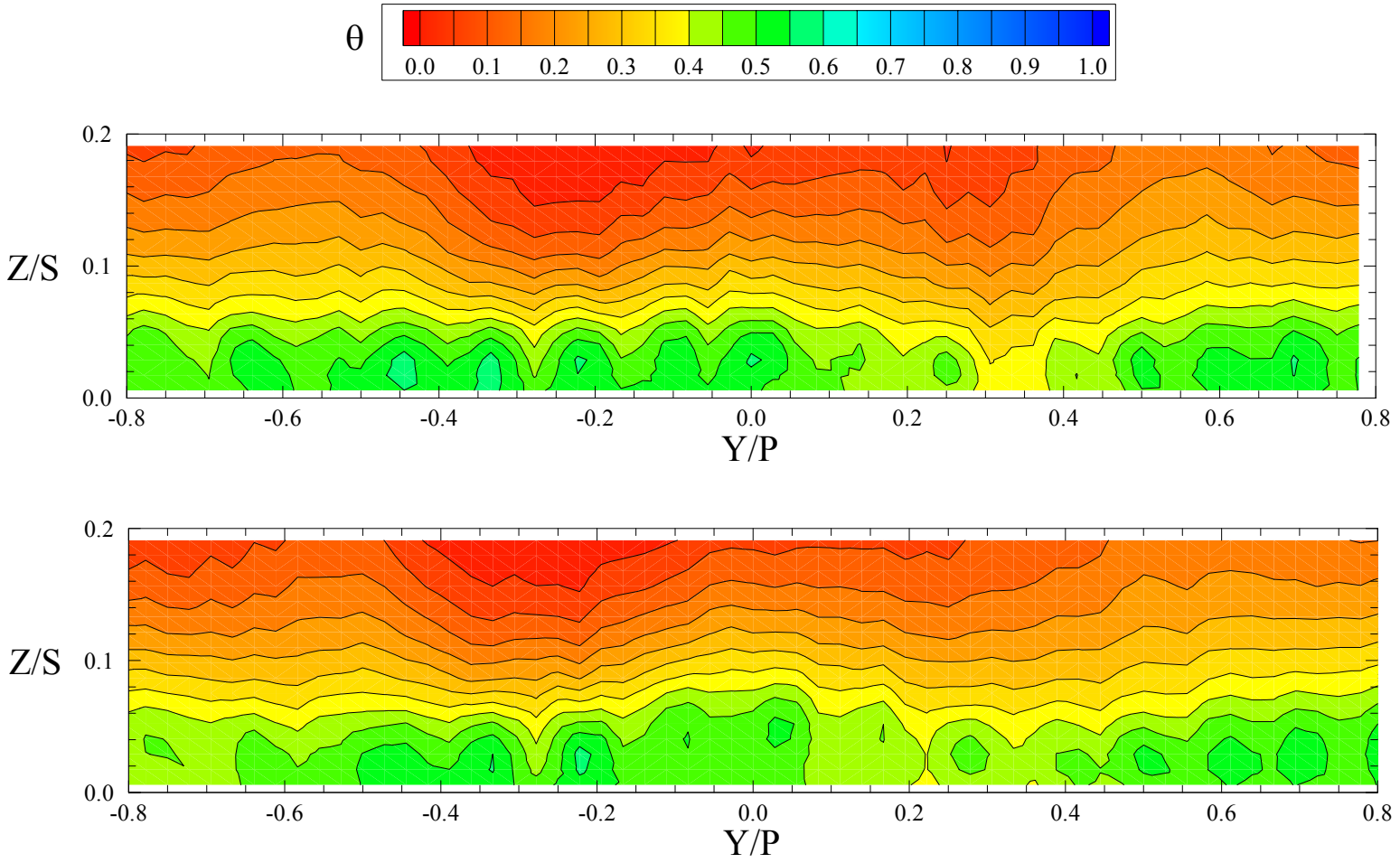

Figure 6.11 Measured inlet near-wall temperature distribution without (top) and with (bottom) the leading edge fillet for the off-design inlet total pressure profile ($\Delta p_{o,max} \approx 2$). Measurement plane is located approximately 10 hole diameters downstream of the last row of film cooling holes.

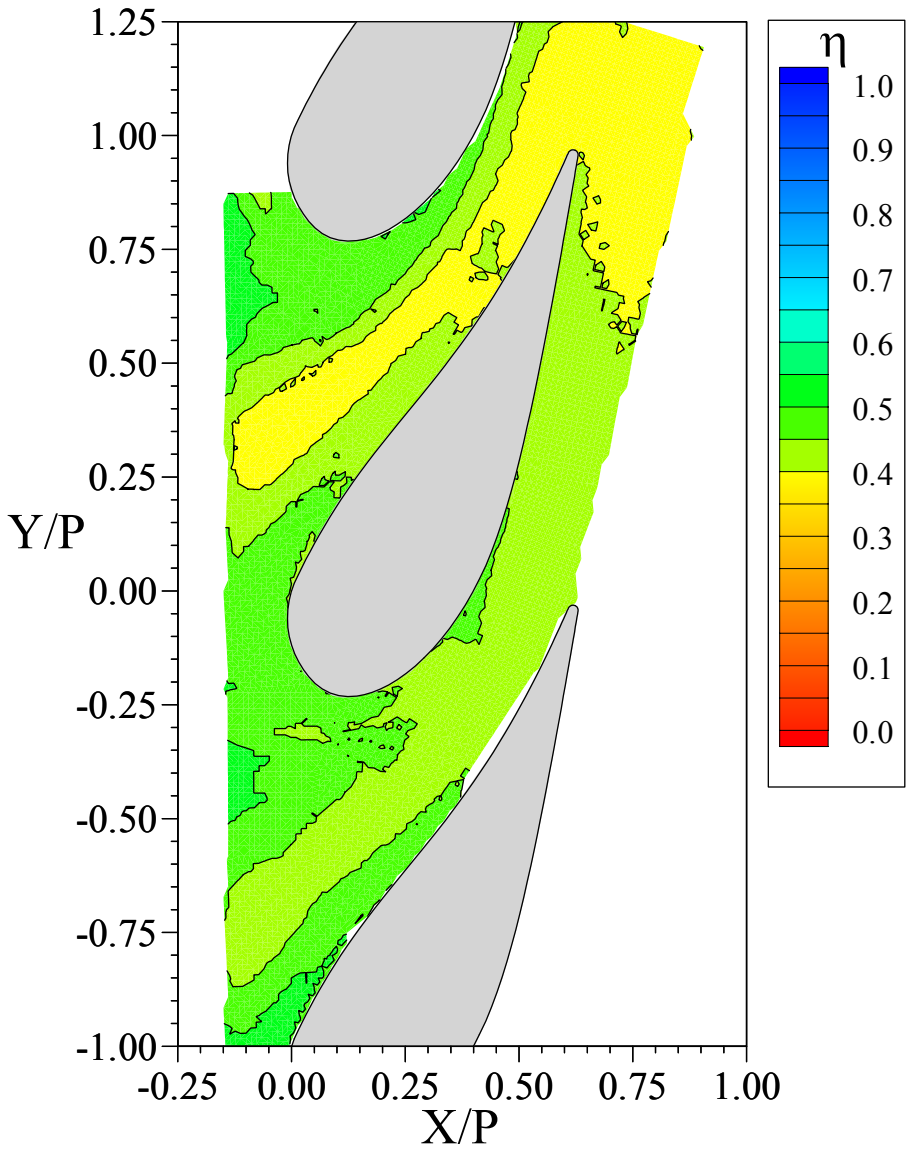

Figure 6.12 Measured endwall adiabatic effectiveness distribution for the baseline, unfilleted vane at the off-design inlet condition ($\Delta p_{o,max} \approx 2$).

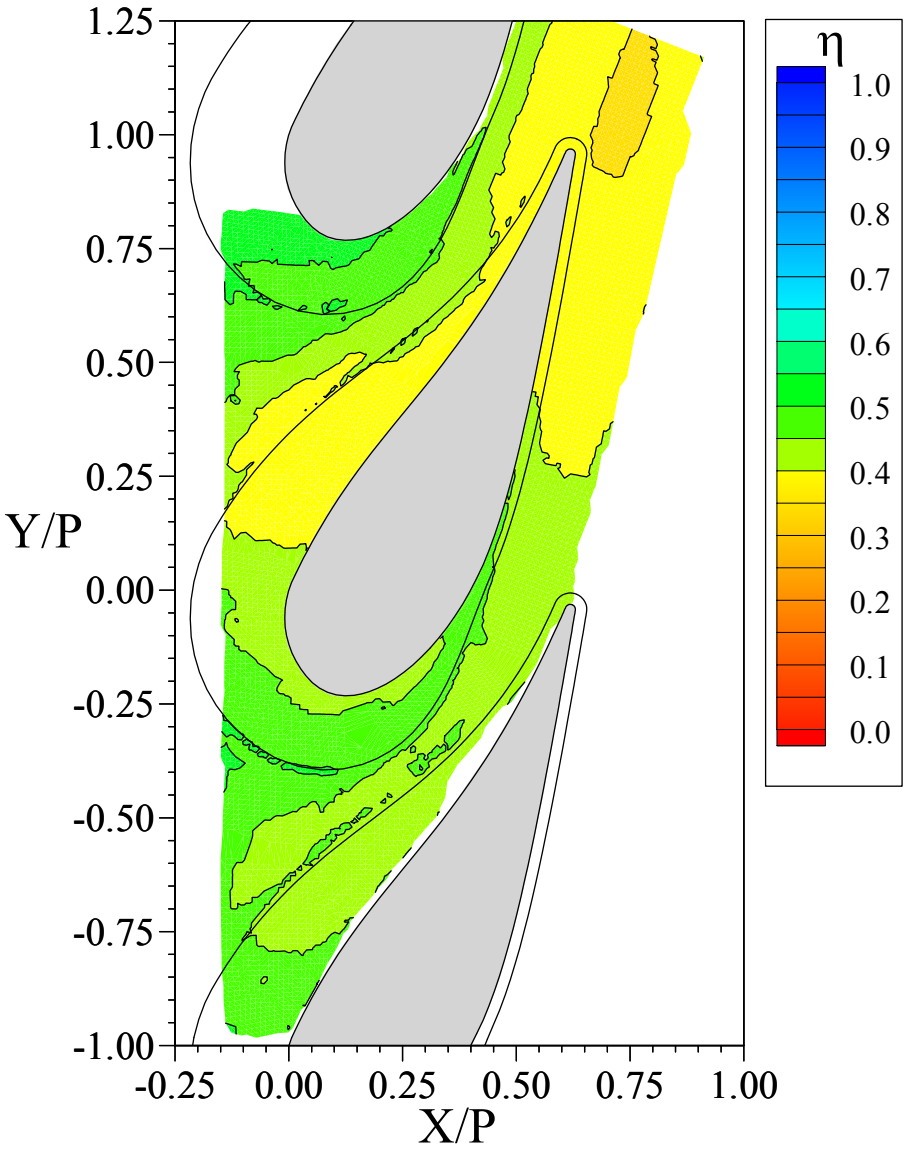

Figure 6.13 Measured endwall adiabatic effectiveness distribution with the fillet at the off-design inlet condition ($\Delta p_{o,max} \approx 2$).

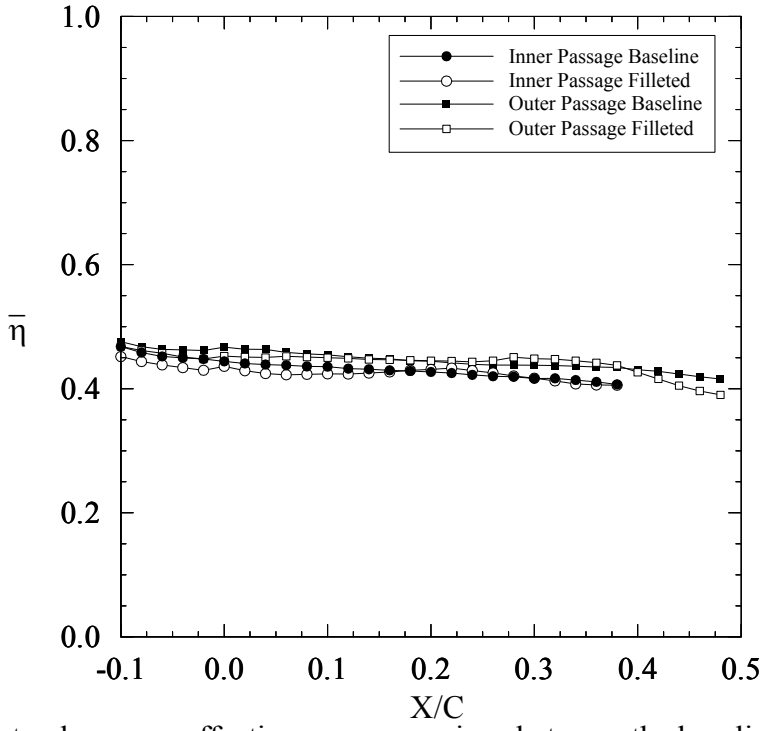

Figure 6.14 Lateral average effectiveness comparison between the baseline and filleted vane for the off-design inlet condition ($\Delta p_{o,max} \approx 2$).

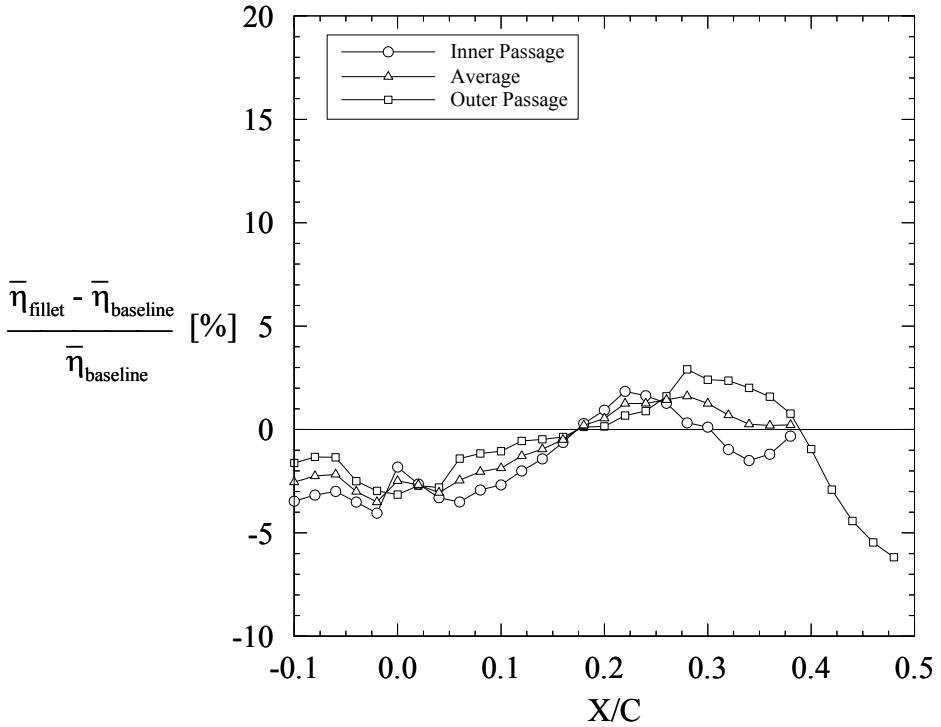

Figure 6.15 Percentage improvement in lateral average effectiveness with the fillet for the off-design inlet condition ($\Delta p_{o,max} \approx 2$).

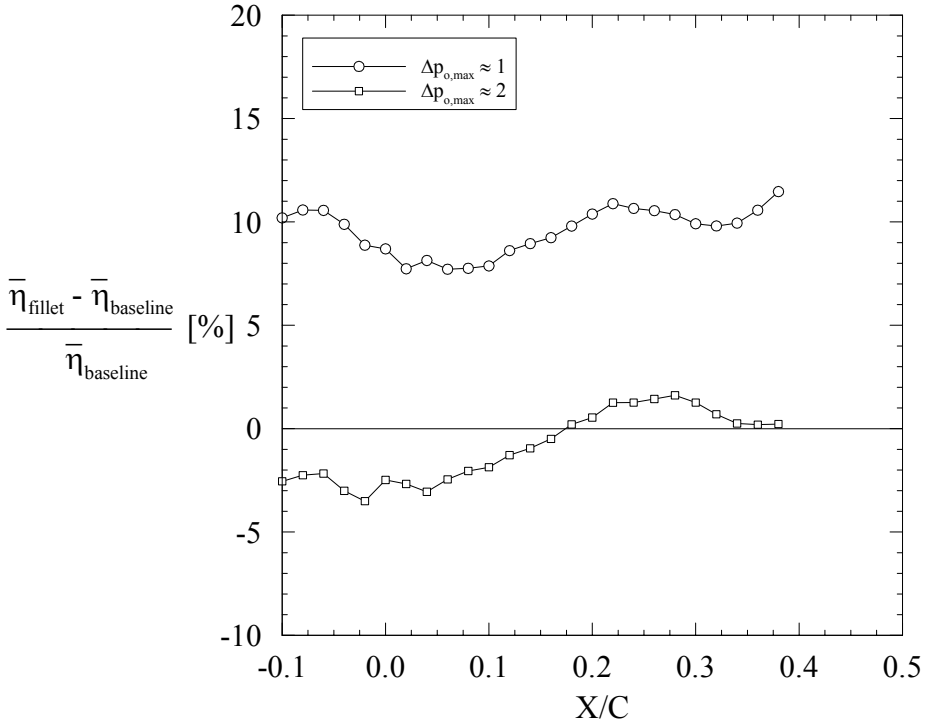

Figure 6.16 Comparison of the average percentage improvement in lateral average effectiveness with the fillet between the design inlet condition ($\Delta p_{o,max} \approx 1$) and off-design inlet condition ($\Delta p_{o,max} \approx 2$).

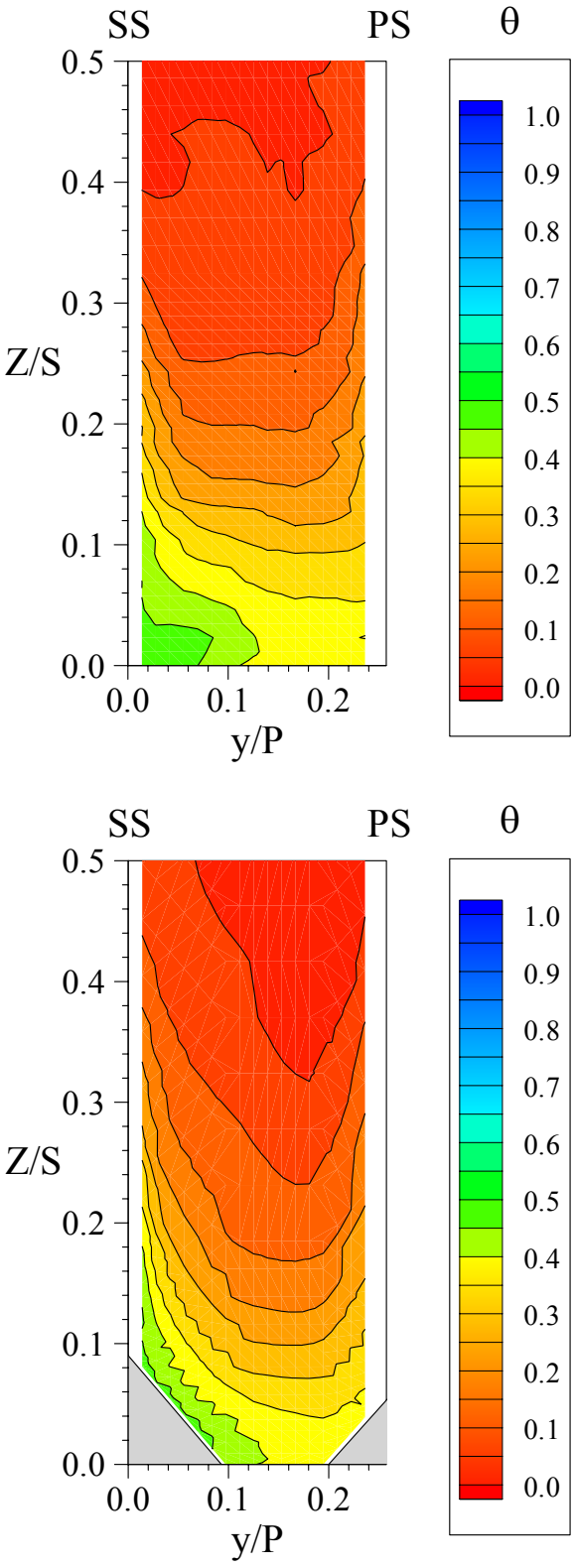

Figure 6.17 Comparison of the thermal field in SS2 between the baseline and filleted vane for the off-design inlet condition ($\Delta p_{o,max} \approx 2$).

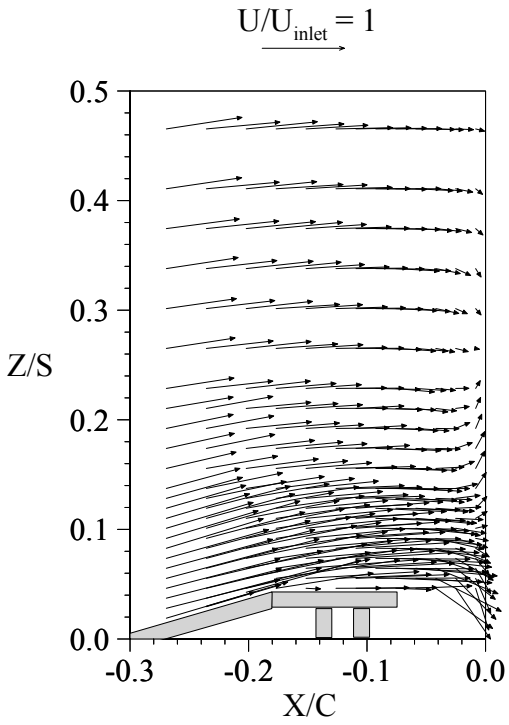

Figure 6.18 Flow field measurements in the leading edge stagnation plane (SP) for the design inlet total pressure profile with backward-facing slot coolant injection.

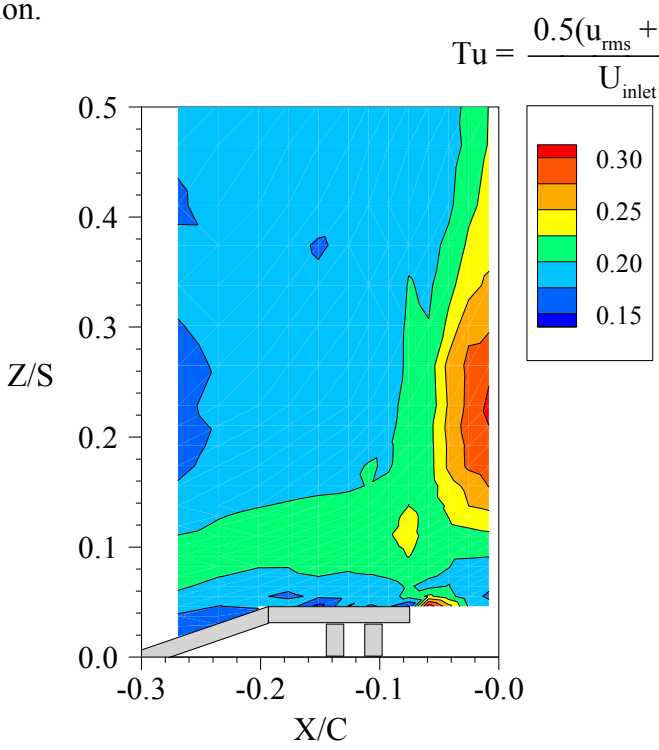

Figure 6.19 Calculated distribution of turbulence intensity in the leading edge stagnation plane (SP).

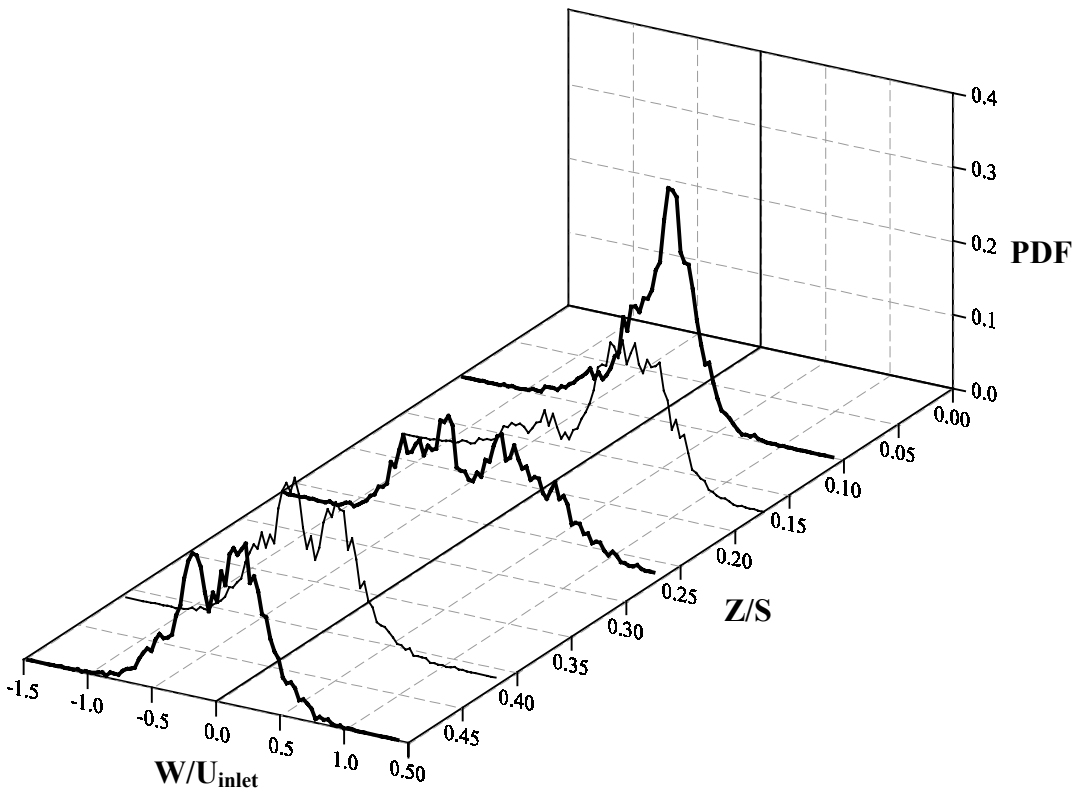

Figure 6.20 Variation of the probability density function (PDF) of W/U_{inlet} with spanwise location along the vane stagnation (X/C = -0.008).

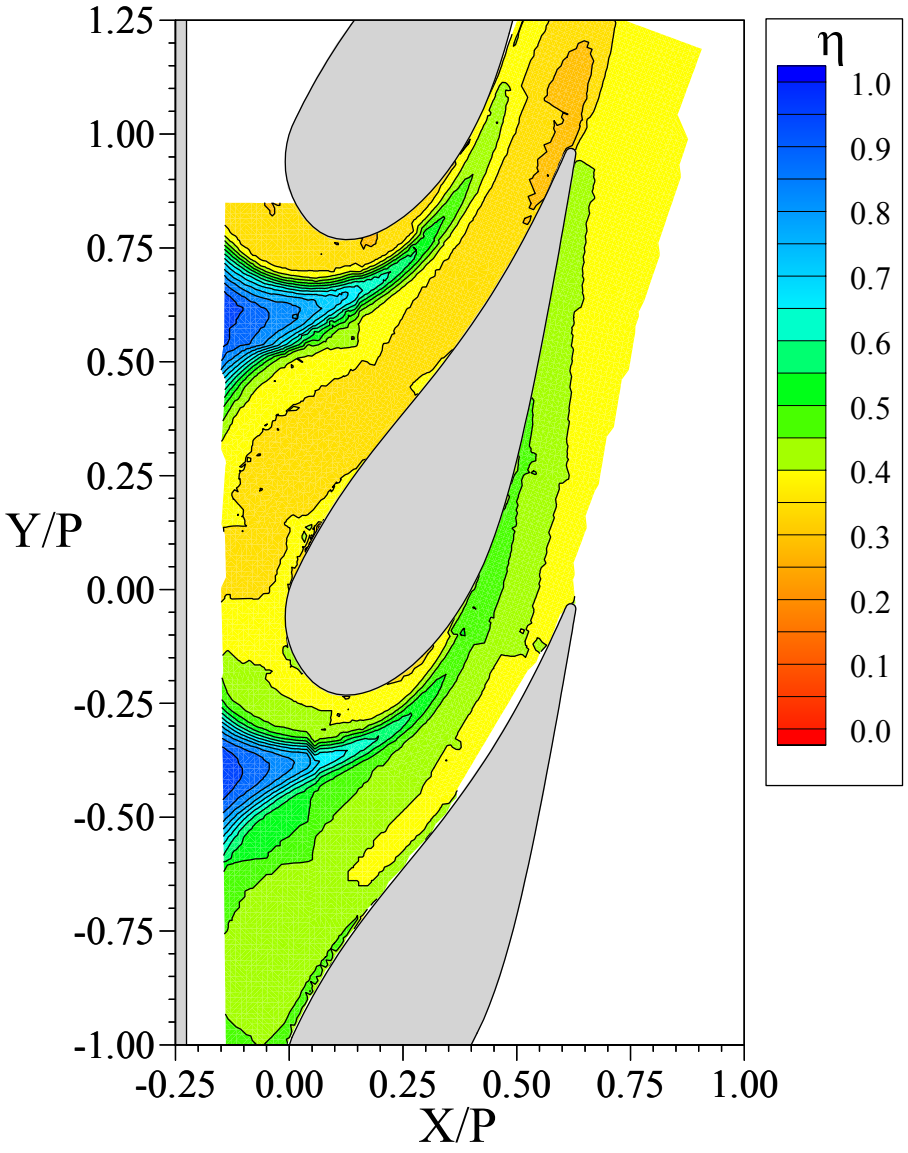

Figure 6.21 Measured endwall adiabatic effectiveness distribution for the baseline, unfilleted vane at the design slot coolant flow rate (0.4%).

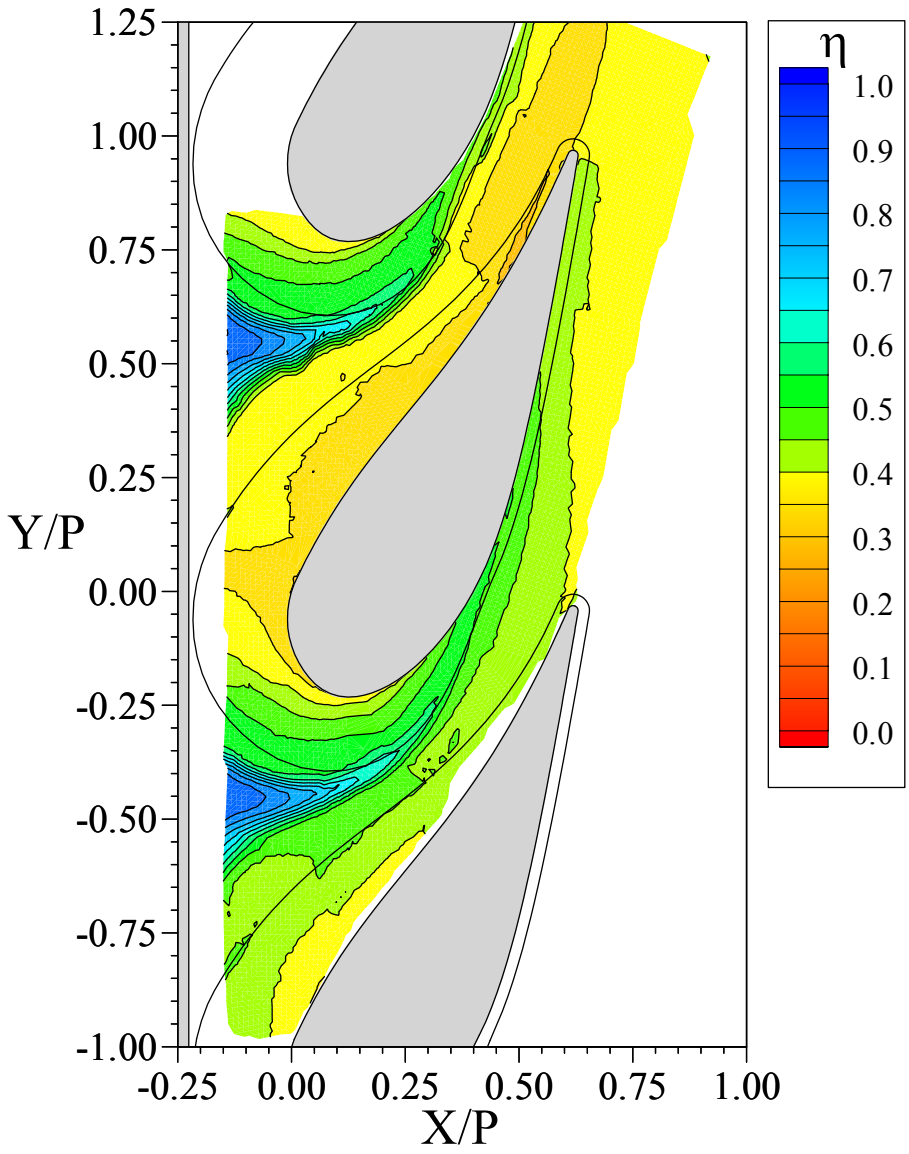

Figure 6.22 Measured endwall adiabatic effectiveness distribution with the fillet at the design slot coolant flow rate (0.4%).

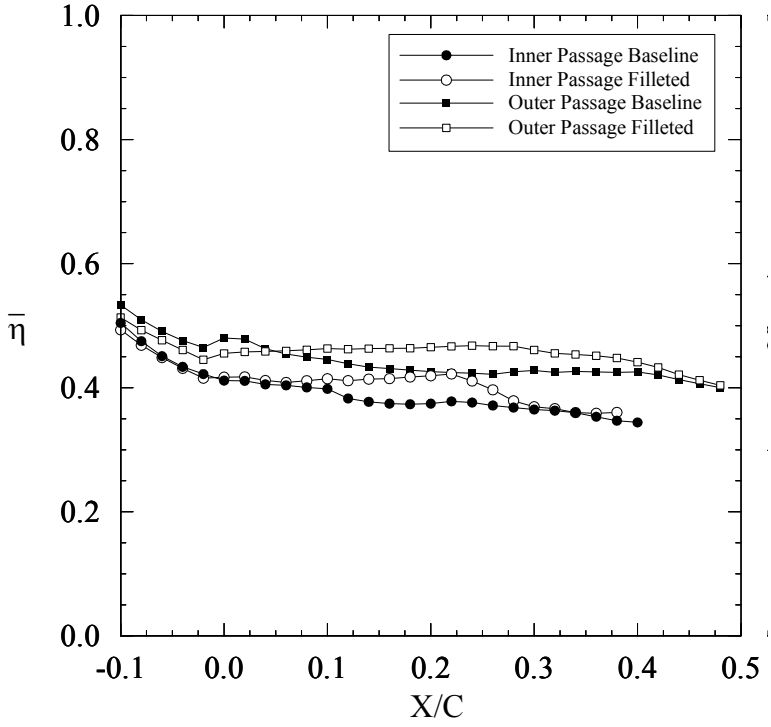

Figure 6.23 Lateral average effectiveness comparison between the baseline and filleted vane for 0.4% slot flow.

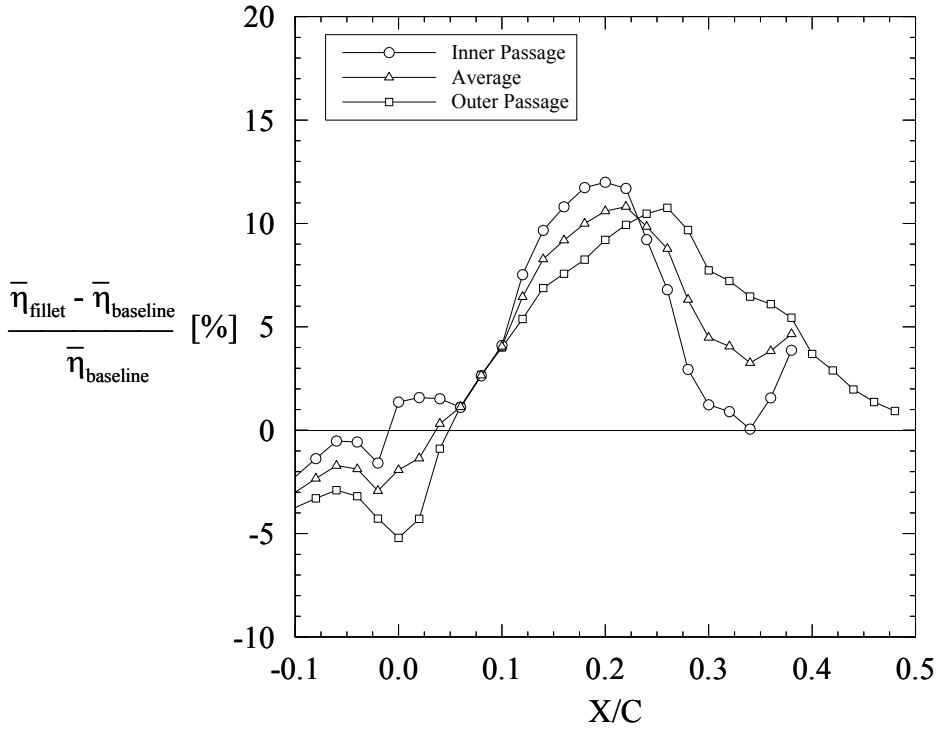

Figure 6.24 Percentage improvement in lateral average effectiveness with the fillet for 0.4% slot flow.

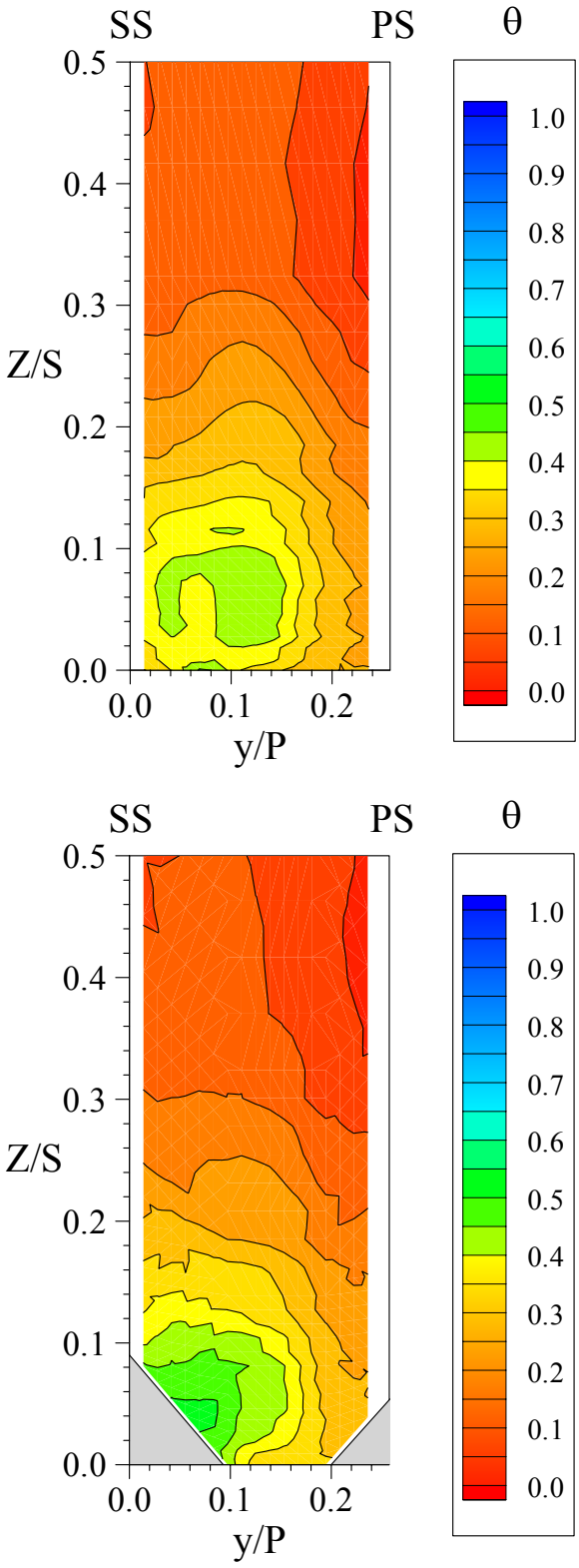

Figure 6.25 Comparison of the thermal field in SS2 between the baseline and filleted vane for the design slot flow rate (0.4%).

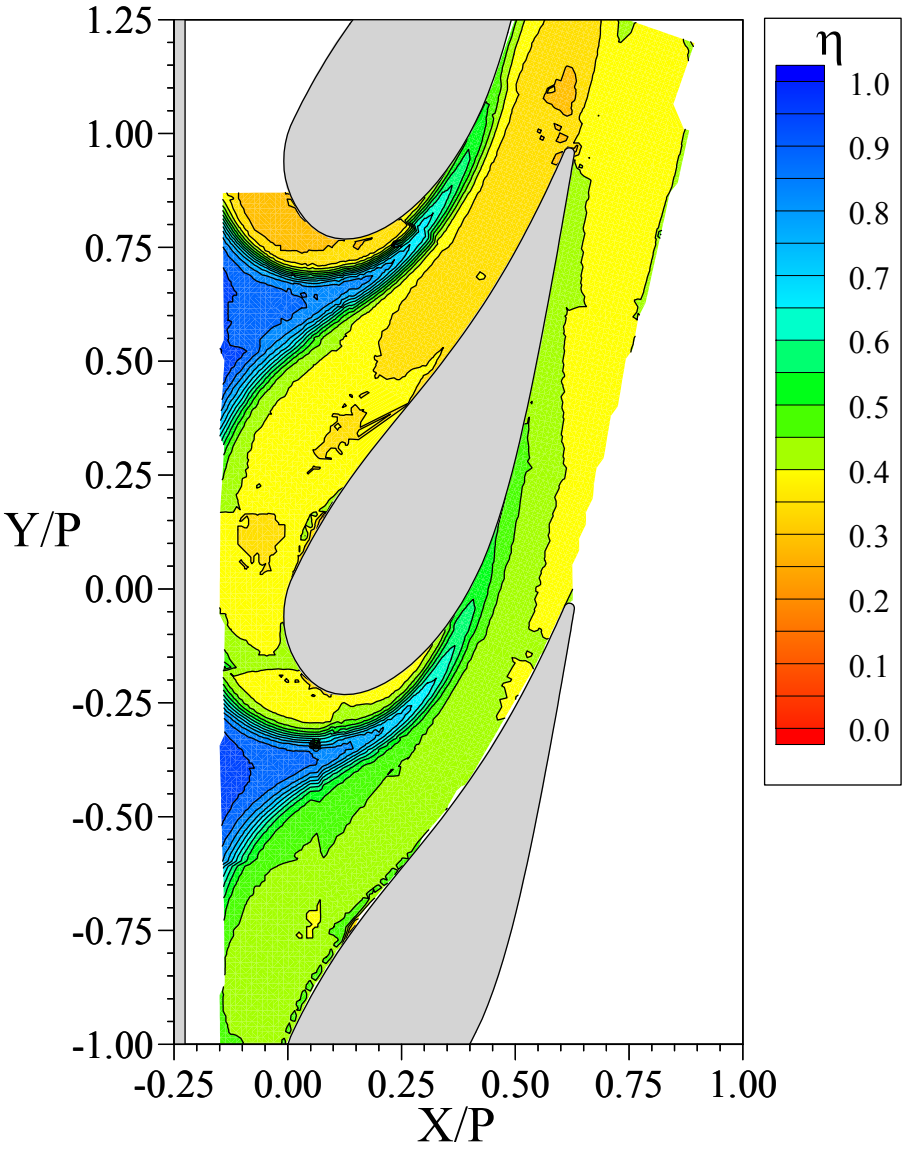

Figure 6.26 Measured endwall adiabatic effectiveness distribution for the baseline, unfilleted vane at the off-design slot coolant flow rate (0.8%).

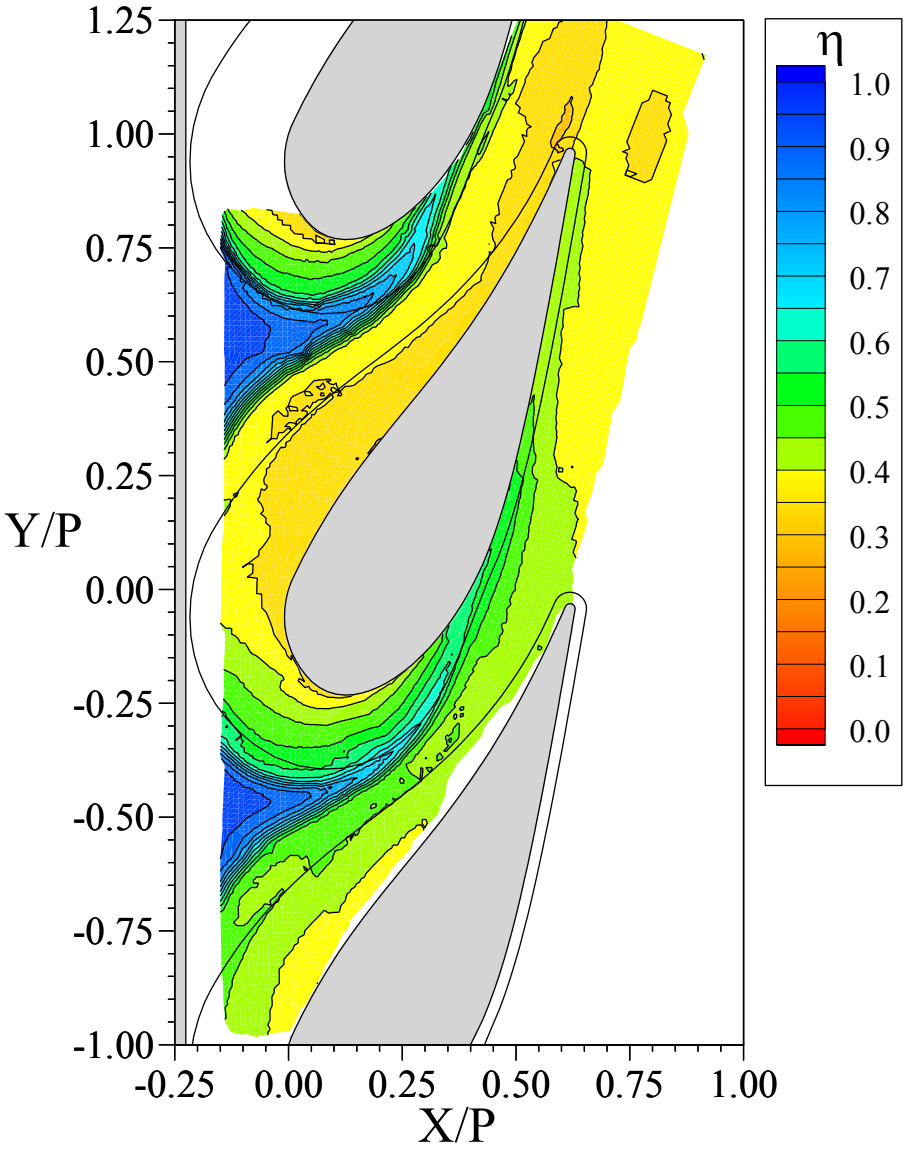

Figure 6.27 Measured endwall adiabatic effectiveness distribution with the fillet at the off-design slot coolant flow rate (0.8%).

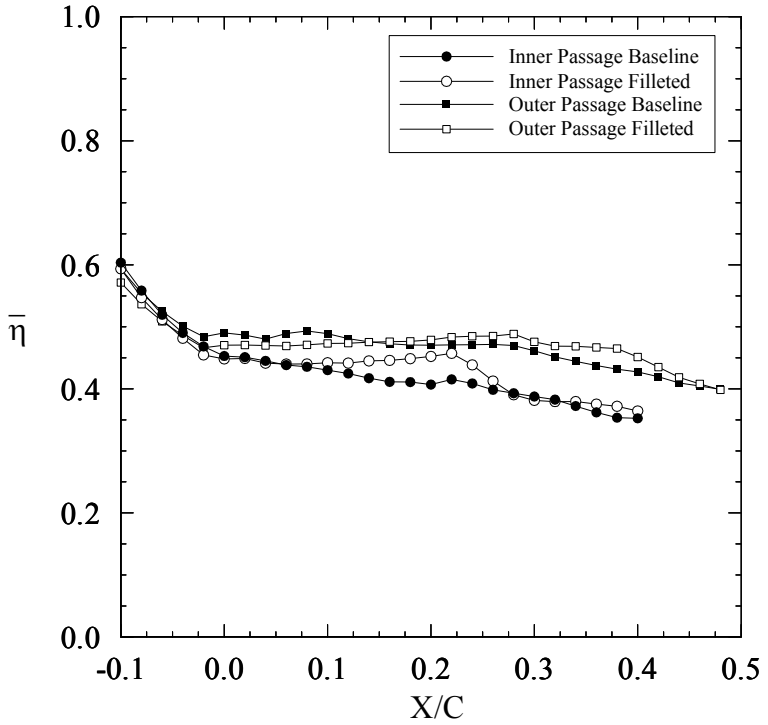

Figure 6.28 Lateral average effectiveness comparison between the baseline and filleted vane for 0.8% slot flow.

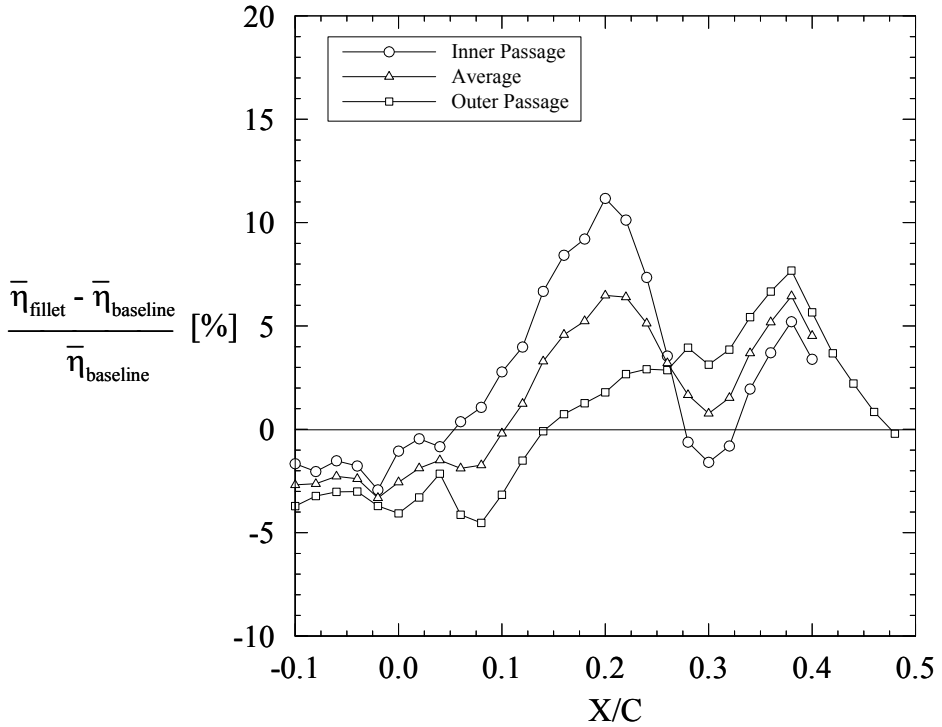

Figure 6.29 Percentage improvement in lateral average effectiveness with the fillet for 0.8% slot flow.

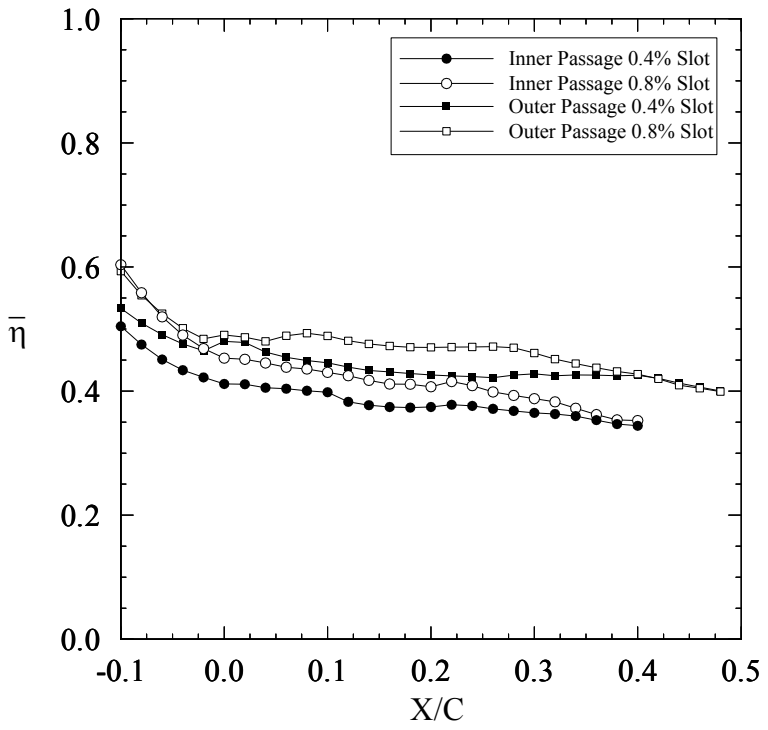

Figure 6.30 Lateral average effectiveness comparison between 0.4% slot flow and 0.8% slot flow without the leading edge fillet.

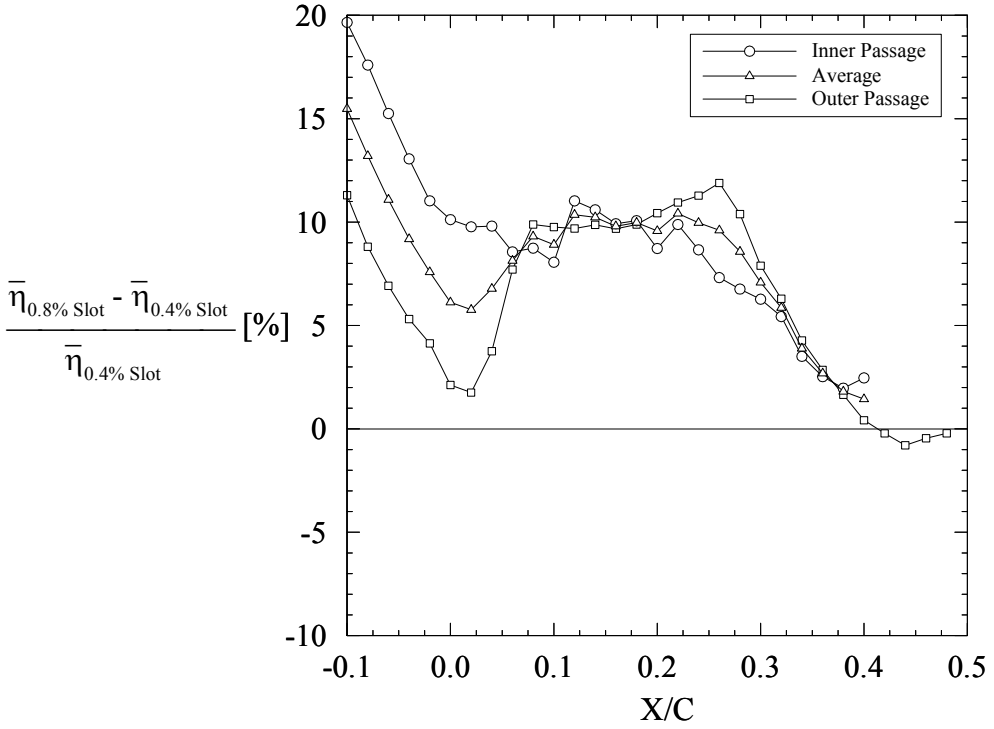

Figure 6.31 Percentage improvement in lateral average effectiveness for 0.8% slot flow versus 0.4% slot flow without the leading edge fillet.

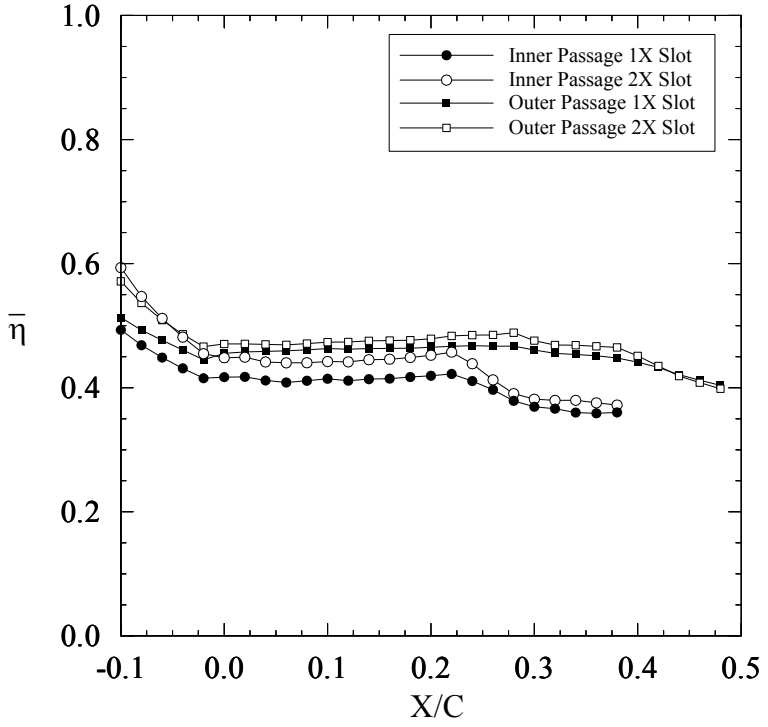

Figure 6.32 Lateral average effectiveness comparison between 0.4% slot flow and 0.8% slot flow with the leading edge fillet.

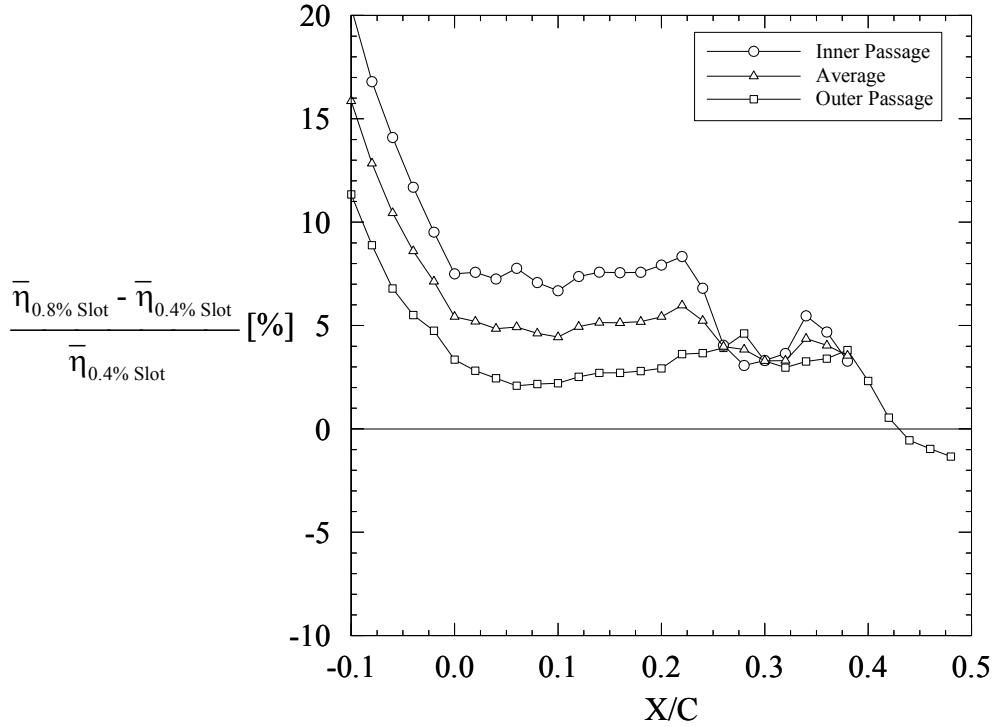

Figure 6.33 Percentage improvement in lateral average effectiveness for 0.8% slot flow versus 0.4% slot flow with the leading edge fillet.

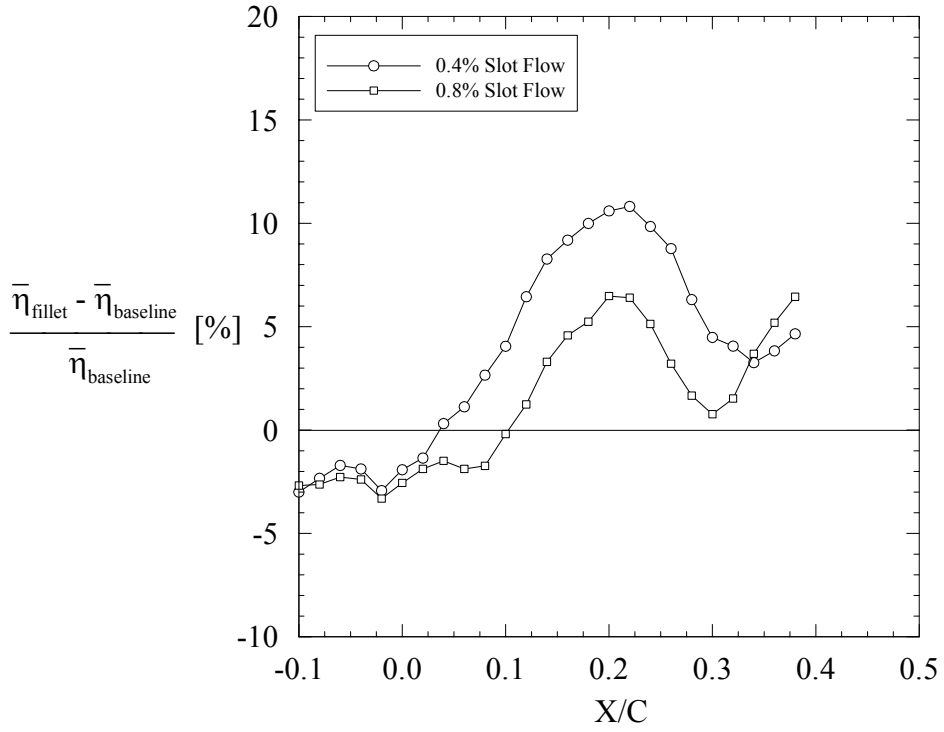

Figure 6.34 Comparison of the average percentage improvement in lateral average effectiveness with the fillet for 0.4% and 0.8% slot flow.

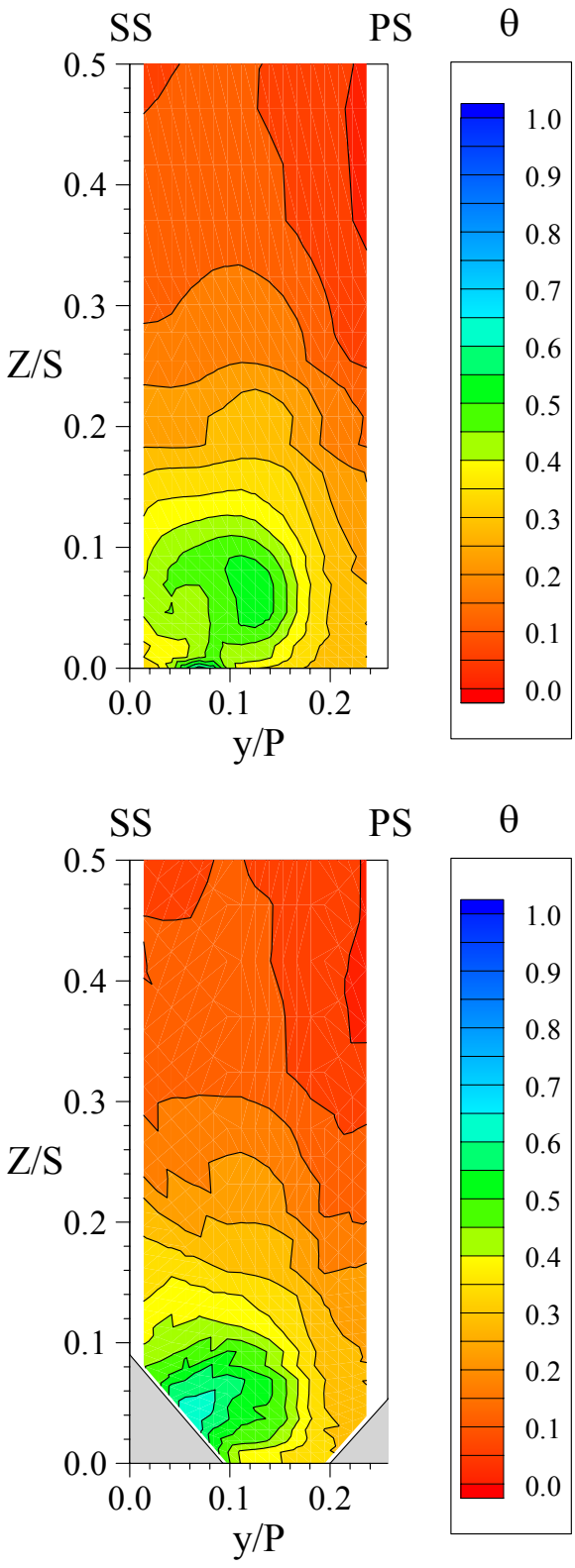

Figure 6.35 Comparison of the thermal field in SS2 between the baseline and filleted vane for the off-design slot flow rate (0.8%).

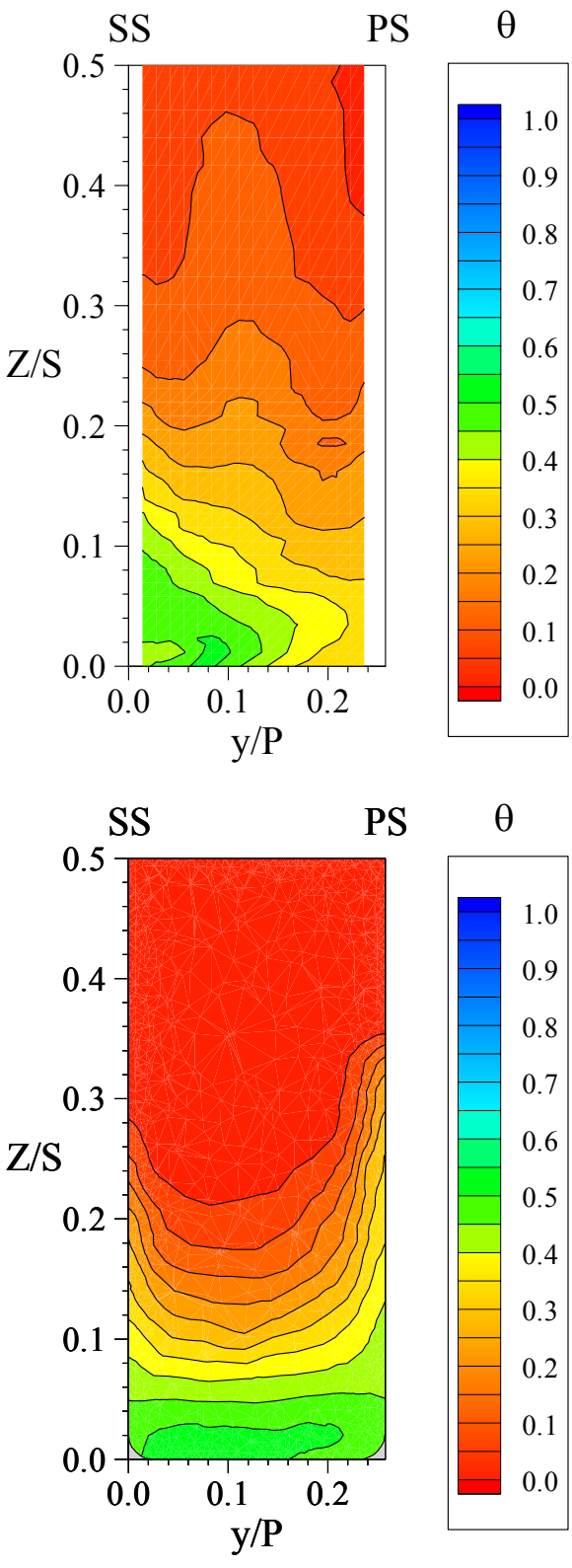

Figure 6.36 Comparison between the measured and predicted thermal fields in SS2 without the fillet at the design inlet condition ($\Delta p_{o,max} \approx 1$).

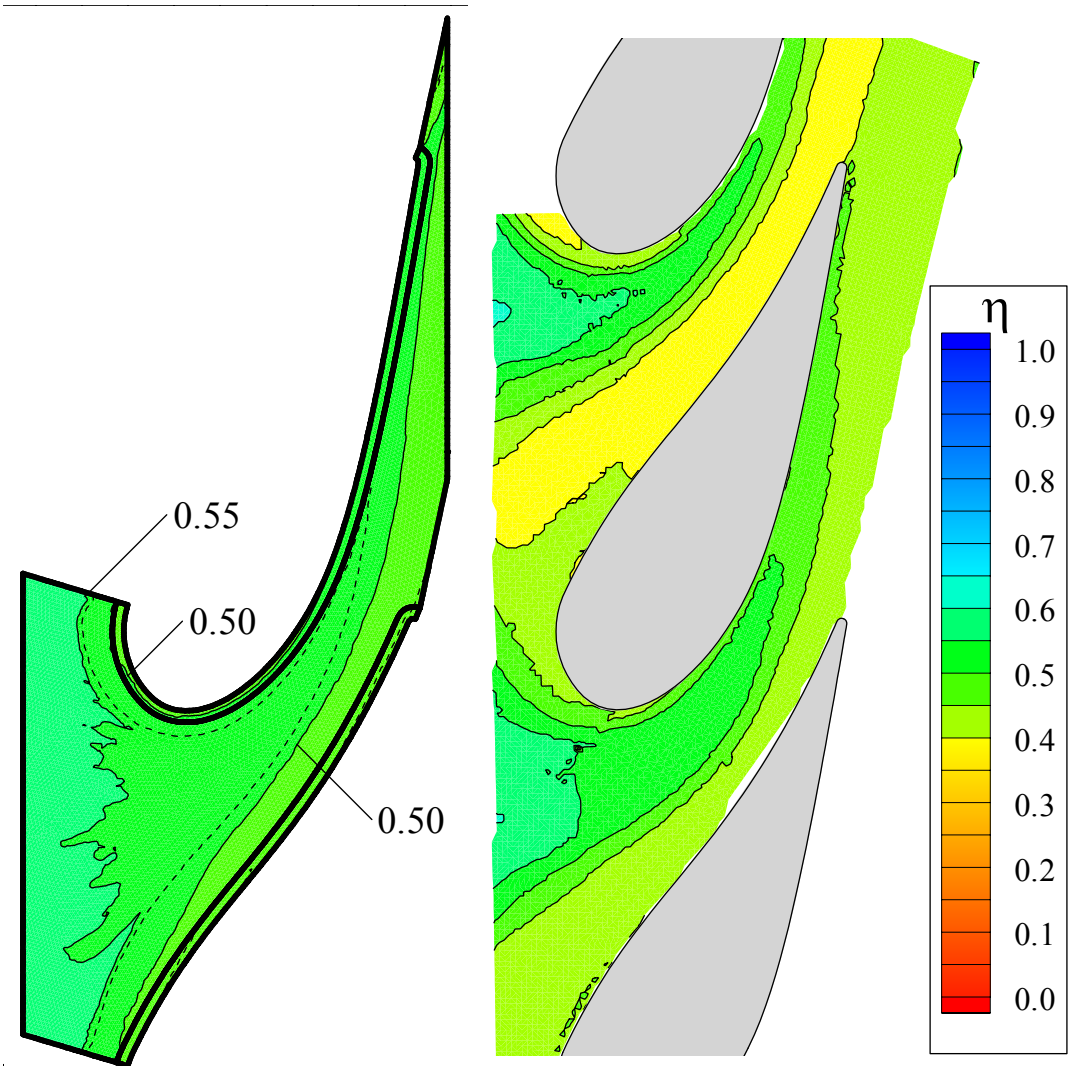

Figure 6.37 Comparison between the predicted and measured distributions of endwall adiabatic effectiveness at the design inlet condition ($\Delta p_{o,max} \approx 1$).

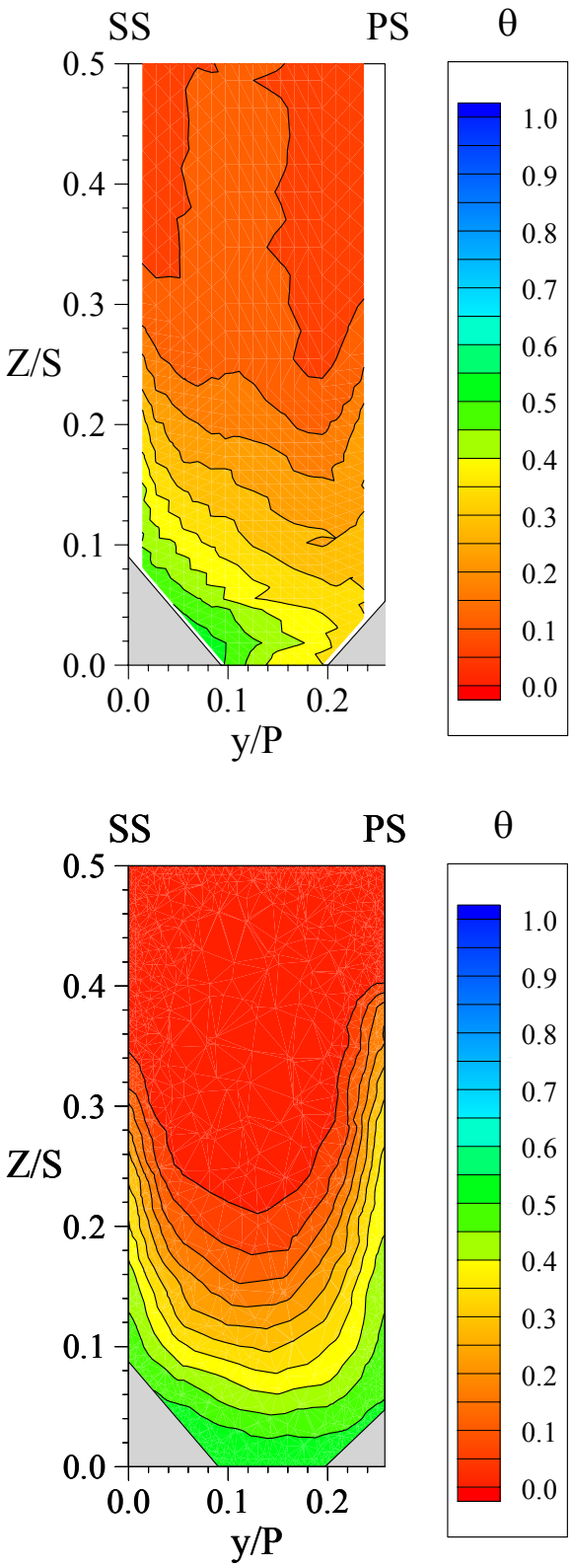

Figure 6.38 Comparison between the measured and predicted thermal fields in SS2 with the fillet at the design inlet condition ($\Delta p_{o,max} \approx 1$).

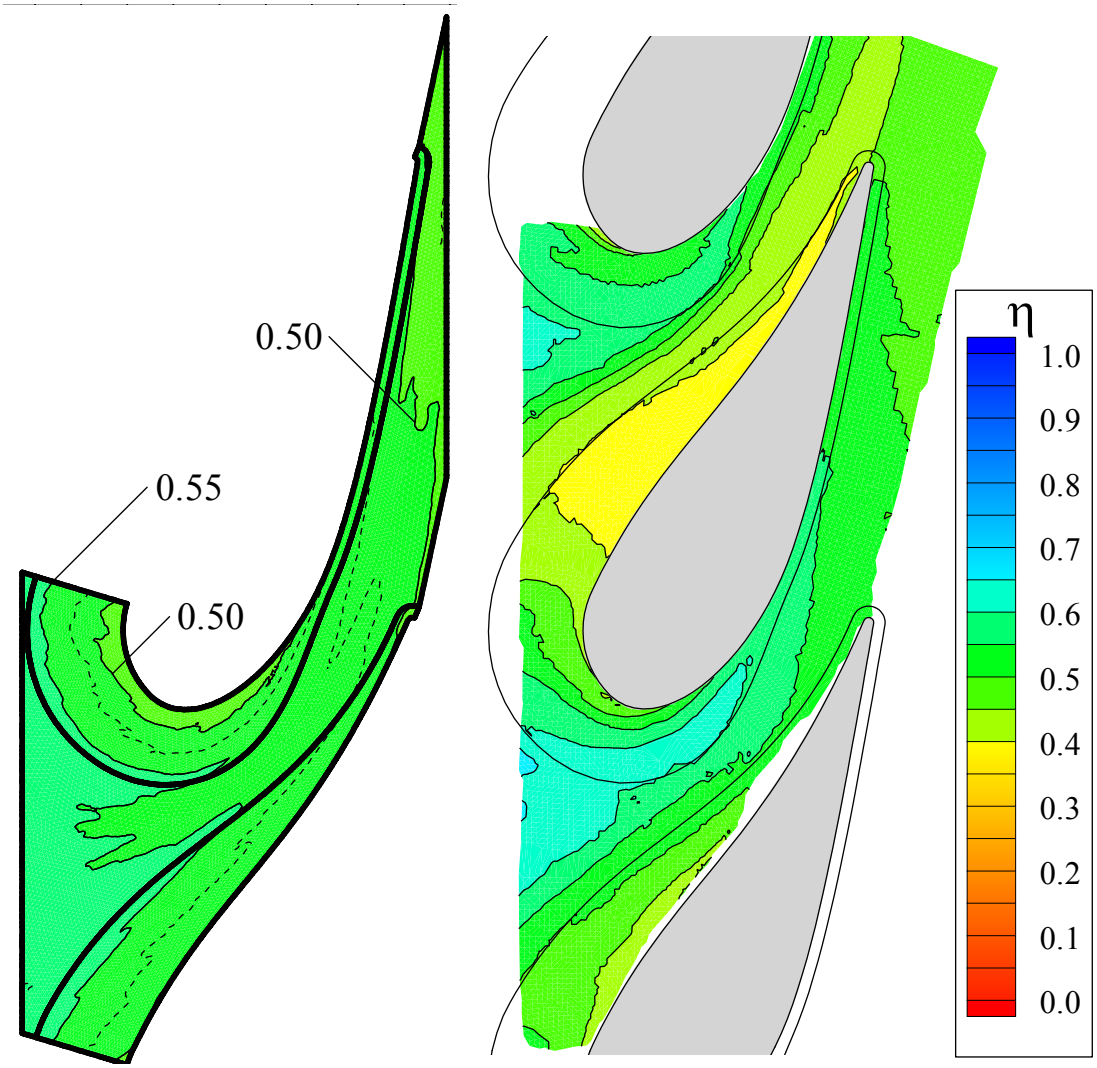

Figure 6.39 Comparison between the predicted and measured distributions of endwall adiabatic effectiveness at the design inlet condition ($\Delta p_{o,max} \approx 1$).

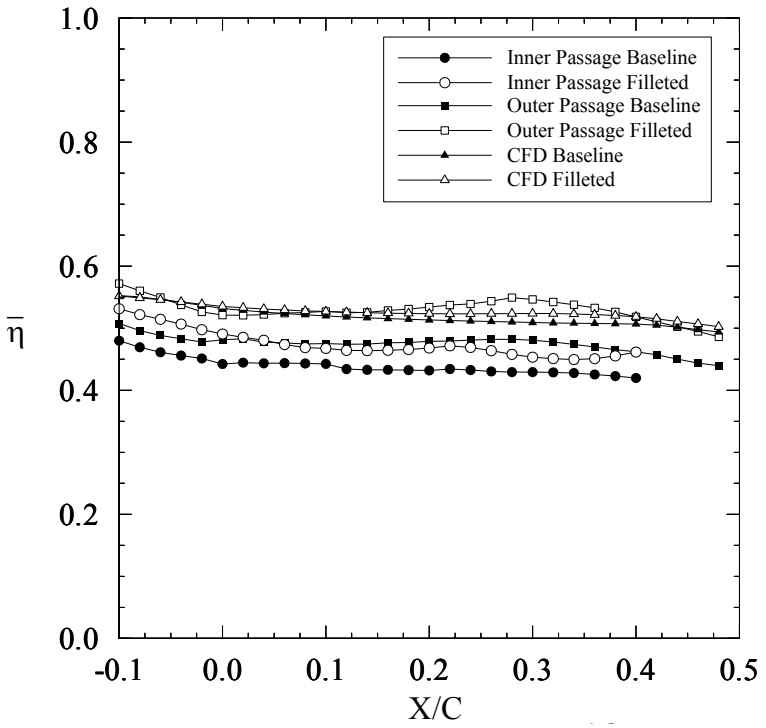

Figure 6.40 Comparison between the measured and predicted distributions of lateral averaged effectiveness for the design inlet condition ($\Delta p_{o,max} \approx 1$).

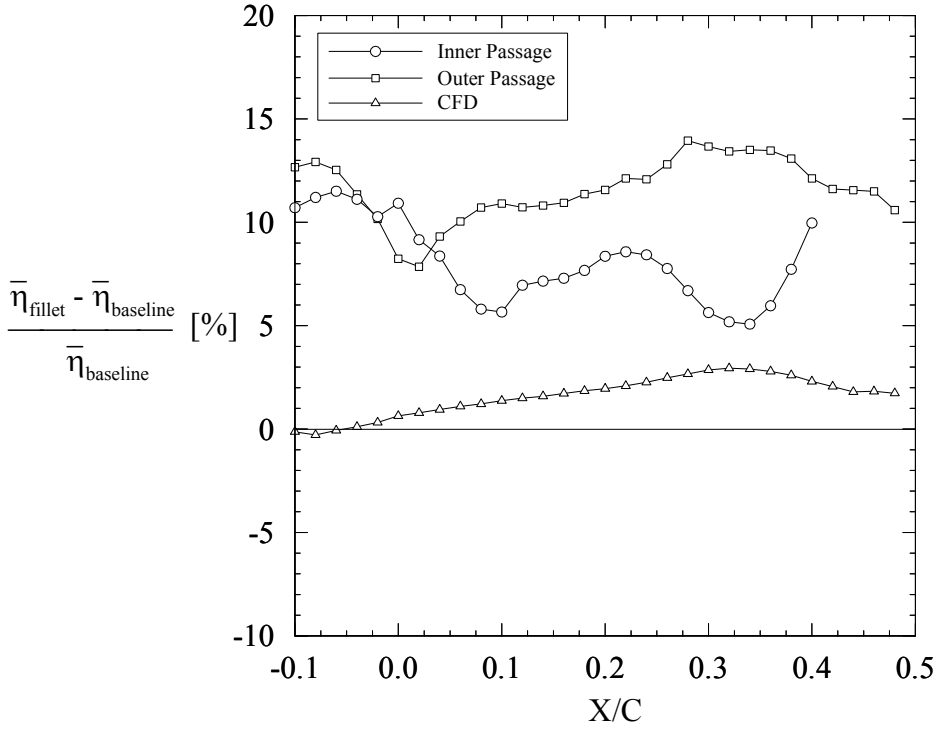

Figure 6.41 Comparison between the measured and predicted percentage improvement in effectiveness for the design inlet condition ($\Delta p_{o,max} \approx 1$).

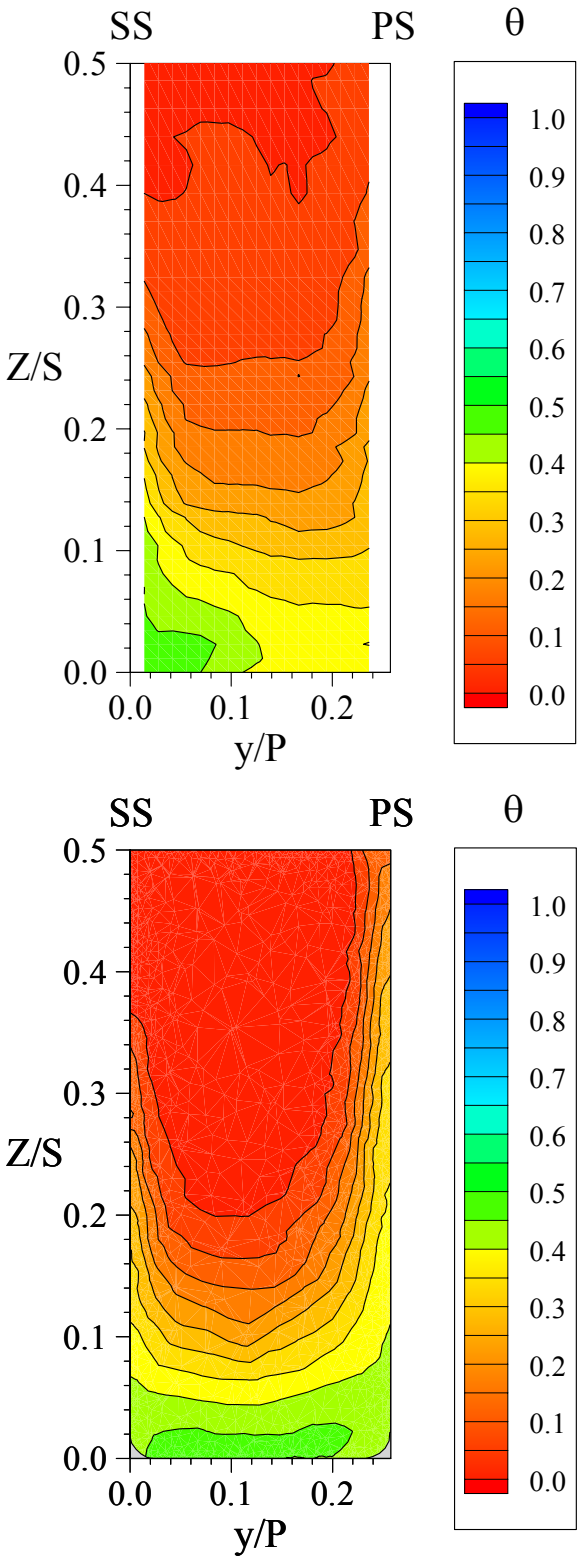

Figure 6.42 Comparison between the baseline measured and predicted thermal fields in SS2 without the fillet at the off-design inlet condition ($\Delta p_{o,max} \approx 2$).

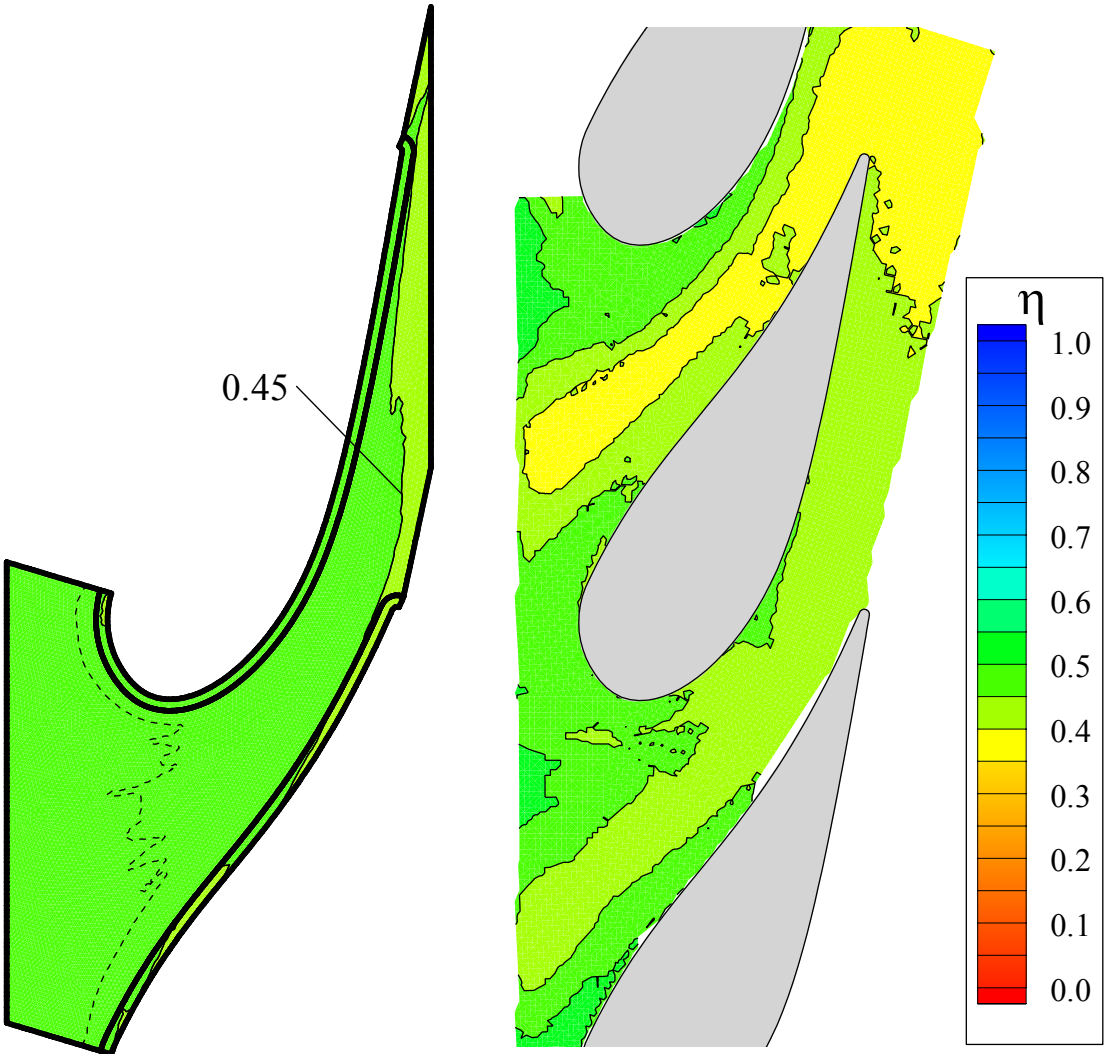

Figure 6.43 Comparison between the predicted and measured distributions of endwall adiabatic effectiveness without the fillet at the off-design inlet condition ($\Delta p_{o,max} \approx 2$).

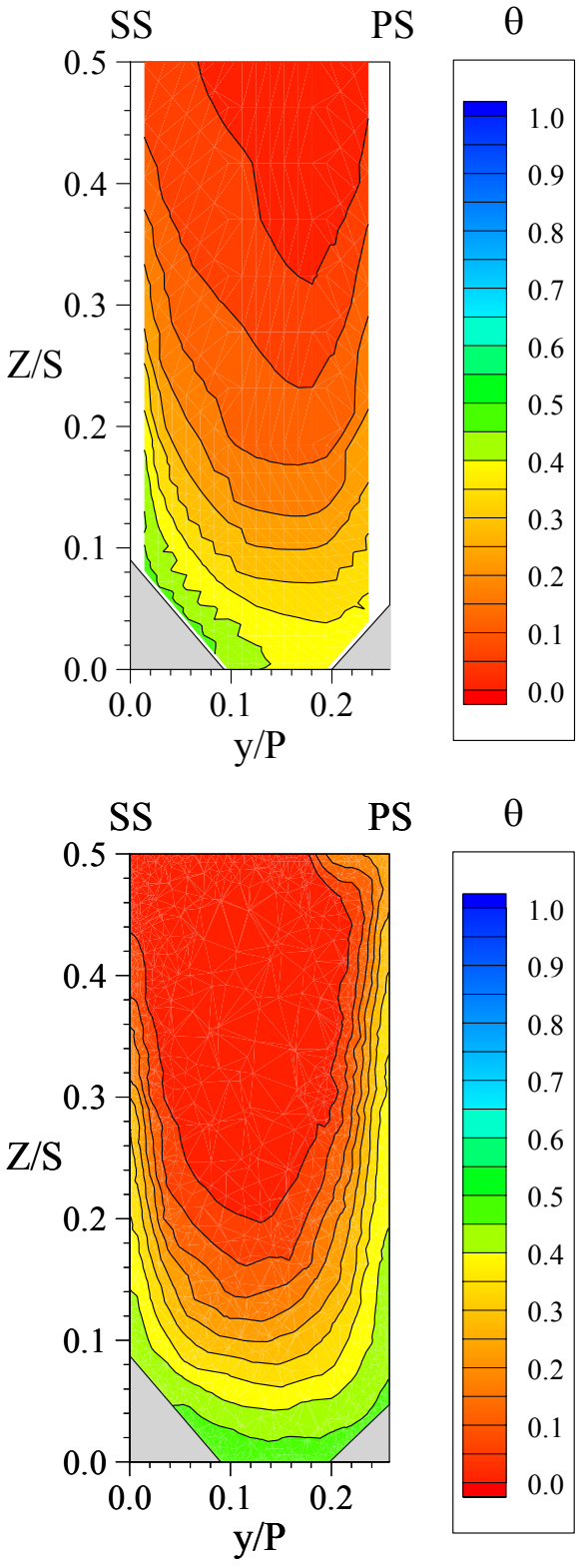

Figure 6.44 Comparison between the measured and predicted thermal fields in SS2 with the fillet at the off-design inlet condition ($\Delta p_{o,max} \approx 2$).

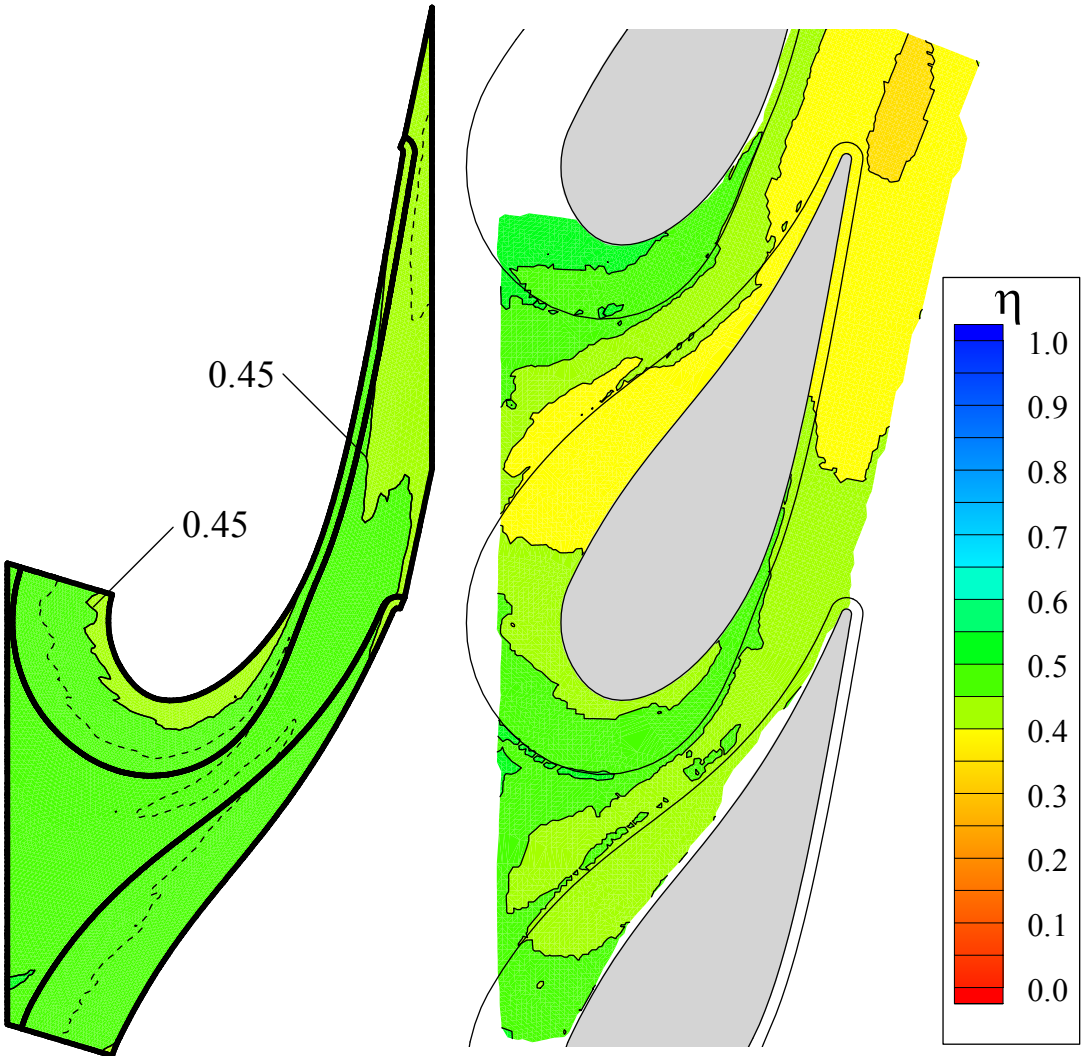

Figure 6.45 Comparison between the predicted and measured distributions of endwall adiabatic effectiveness with the fillet at the off-design inlet condition ($\Delta p_{o,max} \approx 2$).

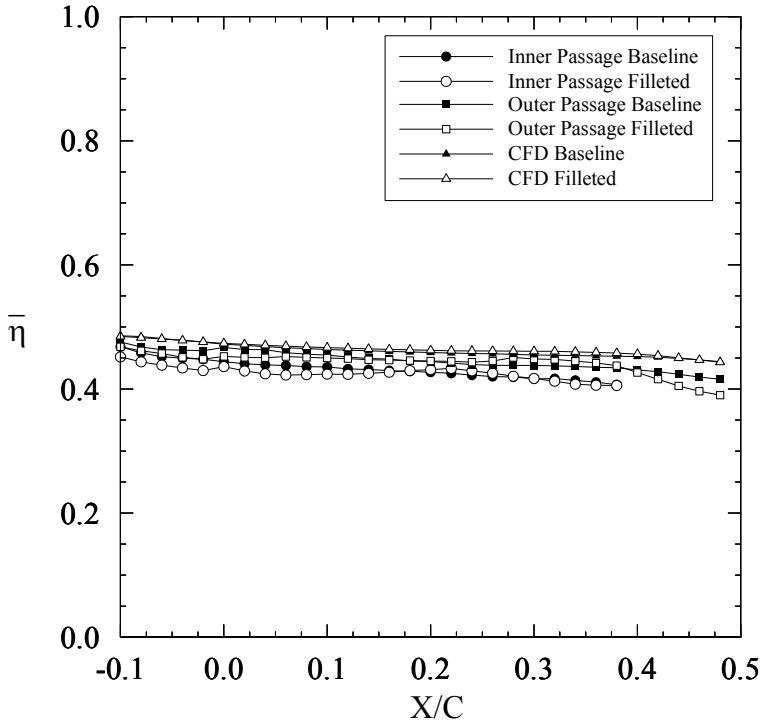

Figure 6.46 Comparison between the measured and predicted distributions of lateral-averaged effectiveness for the off-design inlet condition ($\Delta p_{o,max} \approx 2$).

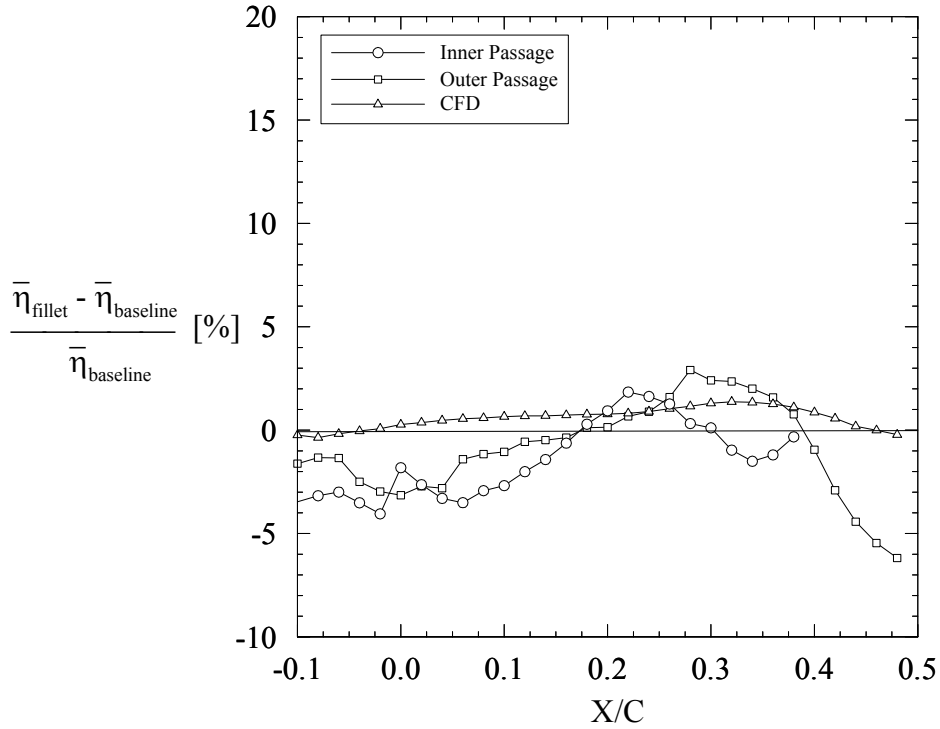

Figure 6.47 Comparison between the measured and predicted percentage improvement in effectiveness for the off-design inlet condition ($\Delta p_{o,max} \approx 2$).

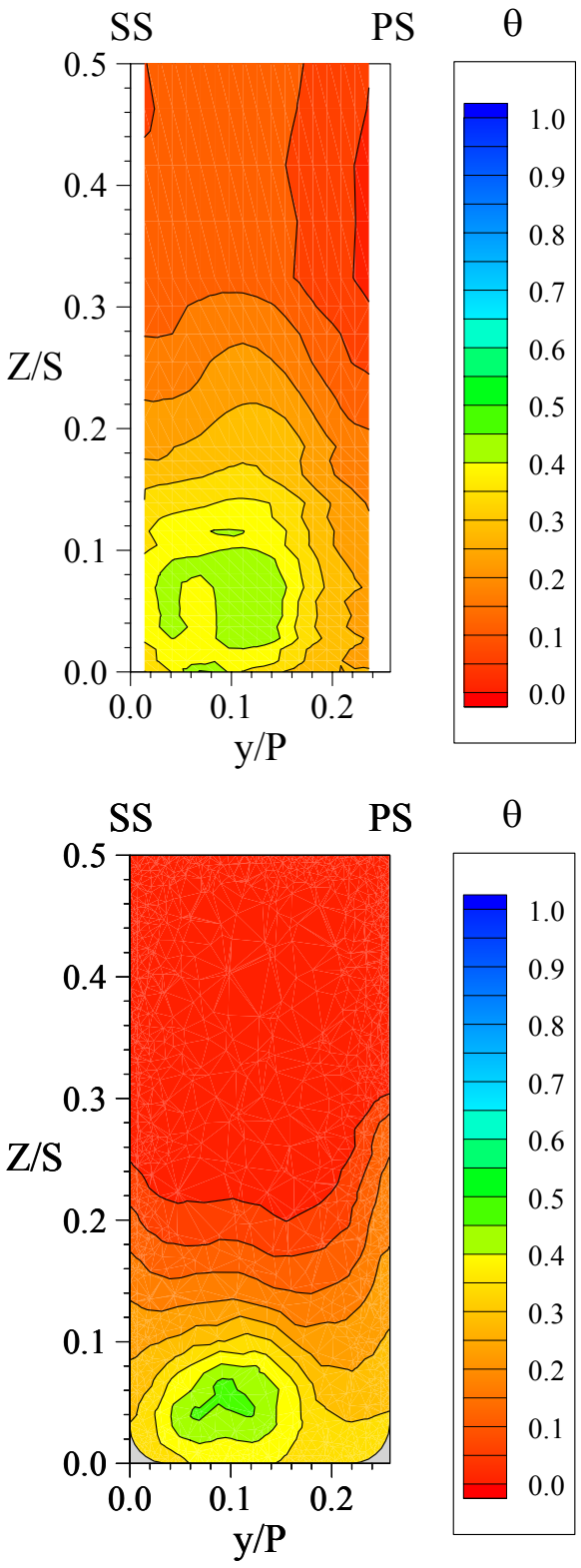

Figure 6.48 Comparison between the measured and predicted thermal fields in SS2 without a fillet for 0.4% slot coolant injection.

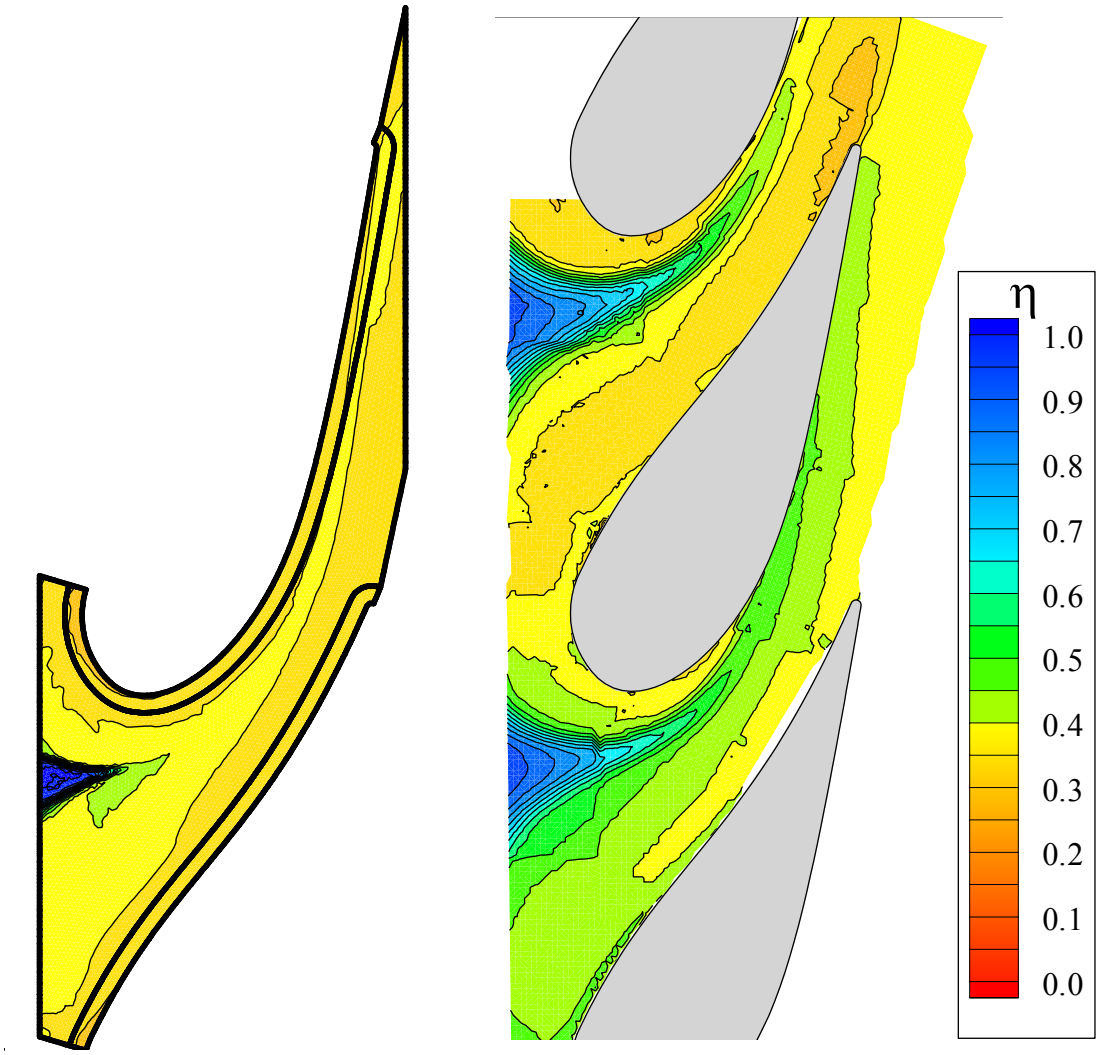

Figure 6.49 Comparison between the predicted and measured distributions of endwall adiabatic effectiveness without a fillet for 0.4% slot coolant injection.

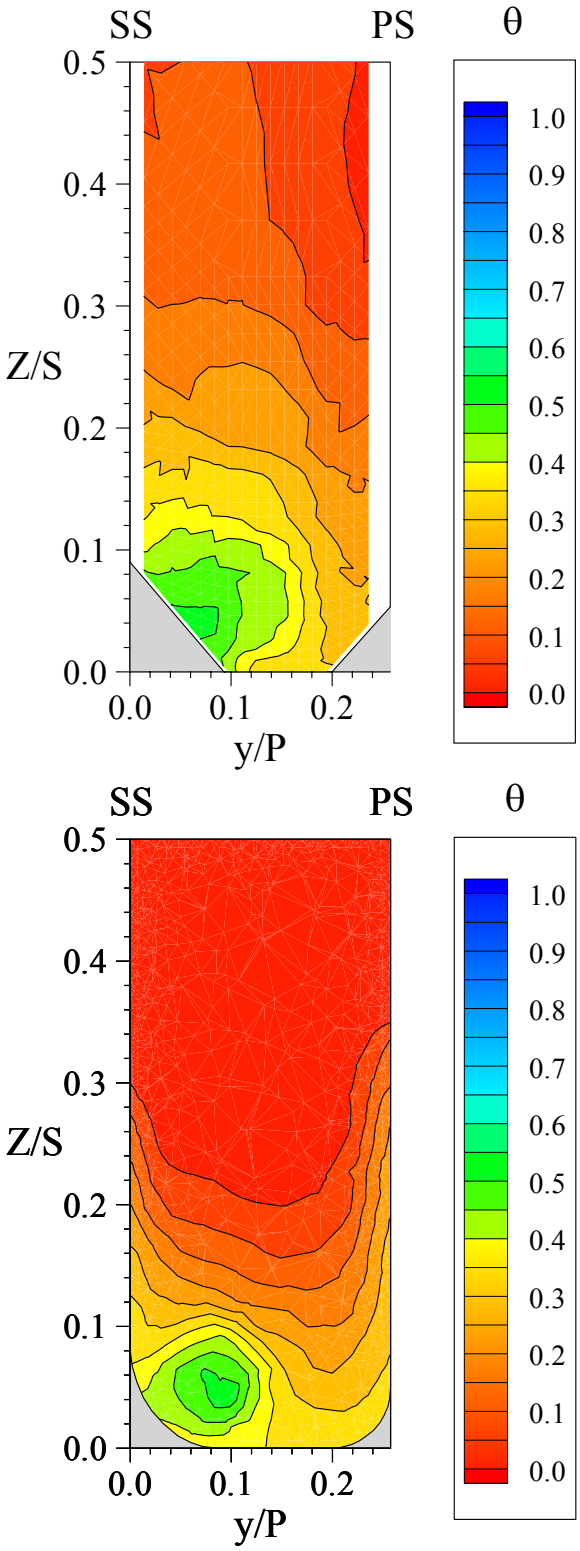

Figure 6.50 Comparison between the measured and predicted thermal fields in SS2 with a fillet for 0.4% slot coolant injection.

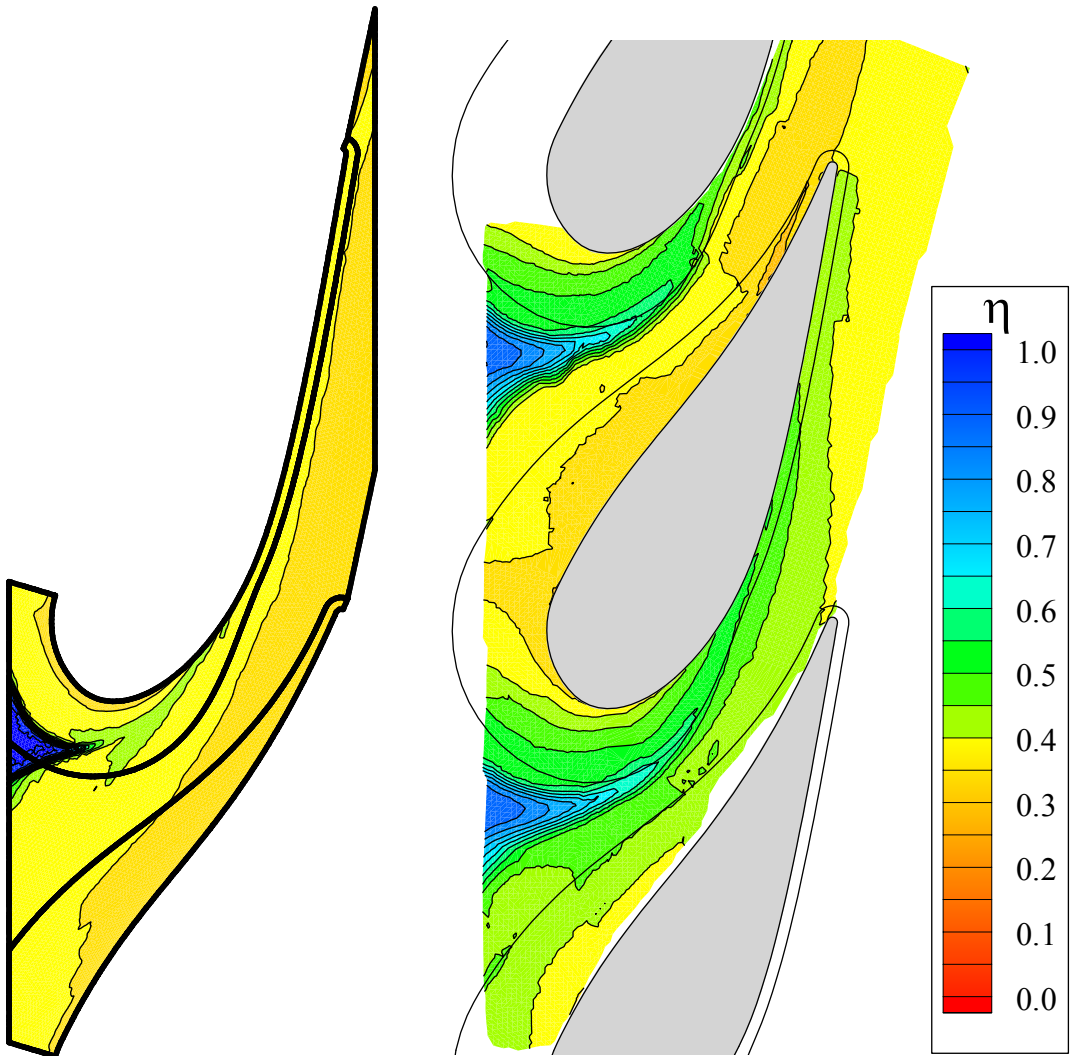

Figure 6.51 Comparison between the predicted and measured distributions of endwall adiabatic effectiveness with a fillet for 0.4% slot coolant injection.